AUTONOMY-AWARE CLUSTERING: WHEN LOCAL DE-CISIONS SUPERSEDE GLOBAL PRESCRIPTIONS

Anonymous authors

000

001

002003004

010 011

012

013

014

015

016

017

018

019

020

021

022

023

024

025

026

027

028

029

031

033

037

038

040

041 042 043

044

045

046

047

048

051

052

Paper under double-blind review

ABSTRACT

Clustering arises in a wide range of problem formulations, yet most existing approaches assume that the entities under clustering are passive and strictly conform to their assigned groups. In reality, entities often exhibit local autonomy, overriding prescribed associations in ways not fully captured by feature representations. Such autonomy can substantially reshape clustering outcomes—altering cluster compositions, geometry, and cardinality—with significant downstream effects on inference and decision-making. We introduce autonomy-aware clustering, a reinforcement (RL) learning framework that learns and accounts for the influence of local autonomy without requiring prior knowledge of its form. Our approach integrates RL with a deterministic annealing (DA) procedure, where, to determine underlying clusters, DA naturally promotes exploration in early stages of annealing and transitions to exploitation later. We also show that the annealing procedure exhibits phase transitions that enable design of efficient annealing schedules. To further enhance adaptability, we propose the Adaptive Distance Estimation Network (ADEN), a transformer-based attention model that learns dependencies between entities and cluster representatives within the RL loop, accommodates variable-sized inputs and outputs, and enables knowledge transfer across diverse problem instances. Empirical results show that our framework closely aligns with underlying data dynamics: even without explicit autonomy models, it achieves solutions close to the ground truth (gap $\sim 3-4\%$), whereas ignoring autonomy leads to substantially larger gaps (\sim 35–40%).

1 Introduction

Clustering, the task of grouping similar entities, underpins a wide range of applications and methodological pursuits, including computer vision, genomics, matrix factorization, and data mining (Karim et al., 2021; Singh & Singh, 2024; Basiri et al., 2025). This process helps reveal the underlying structure of the data and provides insights that can inform decision-making. Formally, given a set \mathcal{I} of N entities, clustering aims to partition them into K clusters by solving

$$\min_{\{\mu(j|i)\},\{C_j\}} \sum_{i=1}^N \rho(i) \sum_{j=1}^K \mu(j|i) \, \Delta(i,C_j), \text{ subject to } \sum_{j=1}^K \mu(j|i) = 1 \, \forall \, 1 \leq i \leq N, \qquad \text{(P1)}$$

where C_j denotes the j^{th} cluster, and $\mu(j|i) \in \{0,1\}$ indicates membership of i^{th} entity in the j^{th} cluster C_j ($\mu(j|i)=1$ if $i \in C_j$, and 0 otherwise). The constraint $\sum_{j=1}^K \mu(j|i)=1$ enforces exclusivity — each entity belongs exactly to one cluster. The cost function $\Delta(i,C_j)$ measures the dissimilarity between entity i and those in cluster C_j , typically defined in terms of feature vectors $\mathcal{X}=\{x_i\}_{i=1}^N$, where $x_i \in \mathbb{R}^d$ represents the attributes of the entity i. The search space of partitions grows combinatorially with N and K, making clustering a computationally challenging problem.

Clustering is also closely related to *resource allocation* problems, such as facility location, data quantization, and graph aggregation (Rose, 1998; Xu et al., 2014). In these problems, the objective is to assign K resources to the entities in \mathcal{I} so that the resources adequately service the entities. This can be viewed as a special case of the clustering problem. For example, the facility location problem can be formulated as $\min_{\{\mu(j|i)\}, \{y_j\}} \sum_{i=1}^{N} \sum_{j=1}^{K} \mu(j|i) d(x_i, y_j)$, where x_i and y_j denote

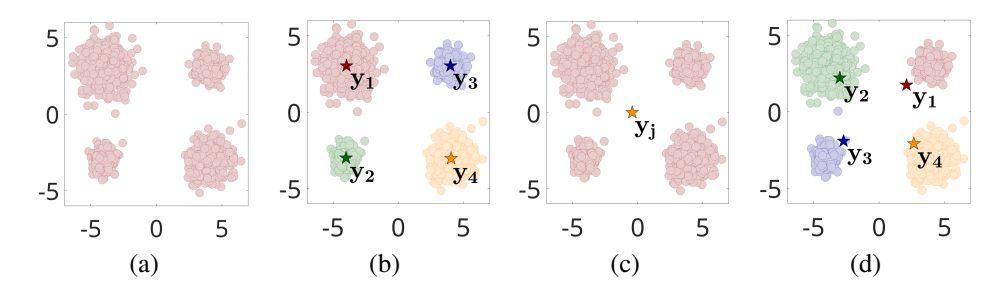


Figure 1: (a) Dataset, (b) No local autonomy - y_j 's at cluster centroid, (c) p(k|j,i) = 0.25, all y_j 's at the centroid of the dataset, and (d) p(k|j,i) = 0.083 if $k \neq j$ and p(k|j,i) = 0.75, y_j 's shifted towards the centroid of the dataset

the feature vectors of the i^{th} client entity and the j^{th} resource facility, respectively. Resource allocation problems can thus be interpreted as clustering tasks in which the dissimilarity function takes the form $\Delta(i, C_j) = d(x_i, y_j)$, with each y_j serving as the feature vector of the representative point (or cluster center) of cluster C_j . Existing techniques in the literature typically treat the entities as passive, meaning that they strictly follow the assignments dictated by the policy μ . However, in many real-world settings, entities exhibit some degree of autonomy, allowing them to override the prescribed assignment and behave as active rather than passive entities. For instance, in decentralized sensing, distributed sensors (entities) are grouped into clusters, each of which communicates its data to an assigned processing unit (resource). Individual sensors, however, may exercise autonomy and transmit their data to a processing unit associated to a different cluster. Such deviations can result from several factors in the network such as signal interference, congestion at the processing unit, energy constraints, or intentional redundancy (Rusu et al., 2018; Yadav & Ujjwal, 2021).

In this work, we introduce the class of autonomy-aware clustering problems, where an entity's cluster membership is determined by two complementary factors: (i) a global assignment policy $\mu(\cdot|i)$, which prescribes the j^{th} cluster for the i^{th} entity when $\mu(j|i)=1$, and (ii) a local autonomy term $p(k|j,i) \in [0,1]$, which probabilistically reassigns the ith entity to the kth cluster given the prescription $j \sim \mu(\cdot|i)$. Existing clustering methods can be seen as a degenerate special case where p(k|j,i) = 1 if k = j and 0 otherwise, strictly enforcing the policy-prescribed assignment without any autonomy. The local autonomy term p(k|j,i) encodes latent behavioral tendencies of entities that are either not captured at all or only partially reflected in the feature vector $x_i \in \mathbb{R}^d$. For example, in decentralized sensing case, x_i may include attributes such as sensor location, recorded data, and current battery charge, but it does not capture network uncertainties such as interference, congestion, or path loss — which are instead reflected through p(k|j,i). Similarly, in recommender systems, a user's feature vector x_i may represent demographic or historical preferences, yet spontaneous choices, mood, or context-dependent behavior are better captured through the local autonomy. This leads to an important observation: while it is often straightforward to construct feature vectors from available information, quantifying local autonomy is considerably more challenging. In practice, this autonomy — driven by an entity's latent behavior — is rarely known explicitly, and this hidden nature constitutes one of the key challenges for autonomy-aware clustering.

The introduction of local autonomy impacts clustering solutions in multiple ways, including altering cluster assignments, cluster sizes and shapes, and the representative feature vectors of cluster centers $y_j \in \mathbb{R}^d$. For illustration, consider the dataset shown in Figure 1(a). Figures 1(b)-(d) depict clustering solutions for different levels of local autonomy. In Figure 1(b), there is no autonomy, and the cluster centers y_j exactly coincide with the respective cluster centroids. In Figure 1(c), the entities have full autonomy: each entity associates itself to each of the four clusters with equal probability, p(k|j,i)=0.25 for all i,j,k. Consequently, all cluster centers $\{y_j\}$ collapse to the centroid of the *entire* dataset. For intermediate levels of autonomy, the cluster centers y_j tend to shift toward the global centroid, increasing accessibility to entities not assigned to them under the policy μ . For example, in Figure 1(d), p(k|j,i)=0.75 if k=j and p(k|j,i)=0.083 otherwise. The algorithm used to generate these solutions is described in Section 3.

Changes in clustering solutions due to local autonomy can significantly affect downstream inference and decision-making. For instance, in decentralized sensing, the cluster center determines the location of the processing unit; with local autonomy, the center is no longer the centroid of the entities assigned to the cluster, but shifts toward the centroid of the entire dataset (see Figure 1(d)).

Similarly, in recommender systems, cluster centers are used to characterize user preference profiles, and shifts induced by local autonomy may lead to different insights for designing new products. Ignoring autonomy, therefore, risks producing misleading conclusions from clustering outcomes.

One of the key contributions of this work is the development of a framework that captures the effect of local autonomy on clustering solutions. The framework is presented in two stages. We first consider the case where the autonomy models are known. Here, we build upon the Maximum Entropy Principle (MEP)—based Deterministic Annealing (DA) algorithm for data clustering (Rose, 1991), which has proven itself to be effective in addressing major challenges such as combinatorial complexity, non-convexity, poor local minima, and sensitivity to initialization. Our reformulation of DA with local autonomy models inherits these advantages. In particular, our modified DA algorithm maintains soft assignment distributions $\pi(j|i) \in [0,1]$, where the annealing parameter β controls the entropy (or "softness") of the assignments. Reformulating the problem in terms of these soft distributions yields explicit solutions for $\pi(j|i)$ at each β , thereby significantly reducing problem complexity. The annealing process, in which these relaxed problems are solved successively as β increases, helps avoid shallow minima and reduces sensitivity to initialization. A key feature of DA is its *phase transition* behavior: cluster centers y_j remain stable over ranges of β and tend to change significantly only at certain critical values. This property enables efficient annealing schedules in which β is increased exponentially.

We then turn to the more practical case where autonomy models are unknown. In this setting, we view clustering as a Markov Decision Process (MDP) with unit horizon: the state space consists of the data points $\{x_i\}$ and cluster centers $\{y_i\}$, the action space corresponds to the set of clusters $\{C_i\}$, local autonomy defines the transition probabilities, the instantaneous cost reflects the clusterassociation cost, and the policy $\mu(j|i)$ specifies the action at each state i. This formulation allows us to leverage reinforcement learning (RL), which can determine cluster assignments without explicit knowledge of the transition probabilities. Accordingly, we propose an RL-based framework that jointly learns both the assignment policy μ and the cluster representatives y_i , effectively tracking the solutions from the known-model case. We develop algorithms for both scenarios: when the local autonomy model p(k|j,i) is independent of the decision variables y_i , and when it depends on them. A further contribution of this work is the Adaptive Distance Estimation Network (ADEN), an attention-based deep model built on a transformer backbone (Vaswani et al., 2017). ADEN enables model-free learning by leveraging the attention mechanism to capture dependencies between entity properties x_i and cluster representatives y_i — dependencies that subsequently determine the assignment policy. Its flexibility in handling inputs and outputs of varying sizes facilitates knowledge transfer across diverse problem instances. Crucially, ADEN takes in the entire set of cluster representatives as input, which is essential to address the scenario where the local autonomy distribution p(k|j,i) depends on all y_i . Such global dependencies are common in applications such as decentralized sensing and recommender systems. The proposed ADEN architecture also allows exploiting hardware parallelism for large-scale datasets.

Empirical evaluations were conducted on a suite of synthetic scenarios where autonomy distributions were governed by scenario parameters, as well as on a decentralized sensing application using the UDT19 London Traffic dataset (Loder et al., 2019), where the problem is posed as optimal UAV placement to maximize coverage of roadside sensors. These studies show that our framework produces solutions that closely reflect the underlying data dynamics: even without explicit autonomy models, the performance of our method on average remains within $\sim 3-4\%$ of modelbased solutions. Interestingly, on some instances of the large-scale decentralized sensing problem, our proposed learning-based algorithm achieves up to a 10% improvement over the case where the local autonomy model is explicitly known, underscoring its inherent capacity to escape poor minima. Note that, the reinforcement learning foundation of our framework equips it with the ability to operate in an online manner, where solutions are not only computed once but can be progressively improved as more information becomes available. This capability is particularly attractive for real-world applications, where data are generated dynamically and the entities have local autonomy.

2 RELATED WORK

Probabilistic model-based clustering has been widely studied in classical machine learning and applied to diverse domains including image segmentation and topic modeling (Deng & Han,

2018). Fundamental approaches include mixture models such as Gaussian Mixture Models (GMM) and Bernoulli Mixture Models (BMM) (McLachlan & Basford, 1988; McLachlan & Peel, 2000; Figueiredo & Jain, 2002; Zhang et al., 2021), as well as algorithms like Expectation-Maximization (EM) (McLachlan & Krishnan, 2008), probabilistic topic models (Hofmann, 2013) and offline/online Deterministic Annealing (Rose, 1998; Mavridis & Baras, 2022). In such frameworks, data points are not deterministically assigned to clusters; instead, they have soft assignments $\pi_{j|i} \in [0,1]$, with $\sum_j \pi_{j|i} = 1$ for each data point i. These soft assignments naturally accommodate stochasticity in cluster assignment at the level of policy, but they do not capture the local autonomy of the agents where they actively choose or reject assignments.

A line of theoretical work in (Harris et al., 2019; Brubach et al., 2024; Negahbani & Chakrabarty, 2021) have formulated clustering directly under stochastic assignment policy and developed approximation algorithms with provable guarantees. For example, (Harris et al., 2019) defines a probability distribution, termed as "k-lottery," over possible sets of K centers rather than deterministically selecting a fixed set. The users however, are still passive recipients of assignments, highlighting a gap between these approaches and applications where agents may autonomously accept or reject assignments. In parallel, researchers have cast clustering as a reinforcement learning (RL) problem. One of the earliest examples is Reinforcement Clustering (RC) (Likas, 1999) where each data point's (assumed passive) assignment to a cluster is treated as an action and the distortion/error acts as the reward signal. More recent work in (Li et al., 2022; Gowda et al., 2022; Zhu et al., 2025), provide a deep reinforcement learning variant of the approach presented in (Likas, 1999).

This line of work also connects to clustering in environments where human behavior introduces uncertainty. For instance, (Banerjee & Veltri, 2024; Ji et al., 2023) highlight how policies assign individuals to behavioral "clusters," yet real-world deviations due to human unpredictability and information asymmetry necessitate probabilistic post-adjustments. Similarly, *The Ethical Algorithm* (Kearns & Roth, 2019) discusses fairness-aware clustering and allocation under uncertainty, underscoring challenges when algorithmic groupings diverge from intended impact.

Unlike prior works, our framework allows stochasticity not only in the cluster-assignment policy but also in the behavior of the entities themselves conditioned on the prescribed cluster. In fact, we explicitly accounts for the latter in the underlying optimization problem that we pose. Building on the DA framework-where the annealing parameter governs the softness of the assignment policy—we introduce a notion of local autonomy: for each entity, a probability distribution governs the realized action conditioned on the assigned policy action. To our knowledge, incorporating such entity-level autonomy into clustering is novel and opens a promising direction for applications where policy adaptation to locally stochastic behavior is essential.

3 Problem Formulation and Solution Methodology

In this article, we modify the classical clustering (resource allocation) problem (P1) to include local autonomy. Let $x_i \in \mathcal{X} \subseteq \mathbb{R}^d$ denote the feature vector of the i-th entity, with relative weight $\rho(i)$ such that $\sum_{i=1}^N \rho(i) = 1$. In the autonomy-aware setting, each entity i may override its prescribed cluster assignment. Specifically, if entity i is assigned to cluster C_j , it may instead select cluster C_k with probability p(k|j,i). The objective is to determine a set of representative feature vectors $\mathcal{Y} := \{y_j\}_{j=1}^K$, corresponding to cluster centers, together with binary association variables $\mu(j|i) \in \{0,1\}$, which indicate the assignment of entity i to cluster C_j , such that the cumulative expected cost of assignment is minimized:

$$\min_{\{\mu(j|i)\},\{y_j\}} \ D := \sum_{i=1}^N \rho(i) \sum_{j=1}^K \mu(j|i) \sum_{k=1}^K p(k|j,i) \, d(x_i,y_k), \quad \text{subject to } \mu \in \Lambda, \qquad \text{(P2)}$$

where $\Lambda = \{\mu : \mu(j|i) \in \{0,1\} \ \forall i,j, \ \sum_{j=1}^K \mu(j|i) = 1 \ \forall i\}$ denotes the set of feasible assignment policies as in (P1). We further define $d_{\mathrm{avg}}(x_i,y_j) := \sum_{k=1}^K p(k|j,i) \ d(x_i,y_k)$ as the average cost of associating the i^{th} entity to the j^{th} cluster.

To address the autonomy-aware clustering problem, we adapt the *maximum entropy principle* (MEP)-based deterministic annealing (DA) algorithm, originally developed for the classical formulation (P1). Instead of solving Problem (P2) directly, we introduce a family of parameterized

problems $(P(\beta))$, which are solved sequentially for an increasing sequence of annealing parameters $\{\beta_k\}$. At each stage, the solution of $(P(\beta_{k-1}))$ is used to initialize $(P(\beta_k))$, and the sequence is constructed such that the limiting solution of $(P(\infty))$ provides a high-quality approximation to (P2).

In $(P(\beta))$ the binary assignment policy $\mu(j|i) \in \{0,1\}$ is relaxed to $\pi(j|i)$, which takes values in the interval [0,1]. This relaxation enables *soft* rather than binary associations, and $\pi(\cdot|i)$ can be interpreted probabilistically as a distribution over cluster assignments for the i^{th} entity. The parameterized problem is then formulated as

$$\min_{\{\pi(j|i)\},Y} F = D - \frac{1}{\beta}H \quad \text{subject to } \pi \in \Lambda_{\beta}, \tag{P(\beta)}$$

where
$$D := \sum_{i=1}^{N} \rho(i) \sum_{j=1}^{K} \pi(j|i) \sum_{k=1}^{K} p(k|j,i) \, d(x_i,y_k), \quad H := -\sum_{i=1}^{N} \rho(i) \sum_{j=1}^{K} \pi(j|i) \log \pi(j|i),$$

denote the relaxed distortion term (corresponding to (P2)) and the conditional entropy of the assignment distribution $p(y_j|x_i)=\pi(j|i)$, respectively. The feasible set is defined as $\Lambda_\beta:=\{\pi:\pi(j|i)\in[0,1]\ \forall i,j,\ \sum_j\pi(j|i)=1\ \forall i\}$, which is the natural relaxation of the feasible set Λ in (P1) and (P2).

The entropy term serves two purposes: (i) it reduces sensitivity to initialization, and (ii) it helps avoid poor local minima. When β is small, the entropy term dominates, encouraging high-entropy (near-uniform) assignments. In this regime, cluster centers $\{y_j\}$ are estimated using information from the entire dataset, producing more global solutions. As β increases, the influence of the distortion term grows, gradually sharpening the assignments towards deterministic clustering. This contrasts with algorithms such as k-means, where cluster centers depend only on local memberships and are therefore highly sensitive to initialization.

For each fixed β , the cost function F is convex with respect to the policy variables $\pi(j|i)$ (although it is not jointly convex in both $\{y_j\}$ and $\{\pi(j|i)\}$). The optimal assignment policy can therefore be obtained in closed form. Specifically, consider the unconstrained Lagrangian $F' = F + \sum_{i=1}^N \nu_i \left(\sum_{j=1}^K \pi(j|i) - 1\right)$, where ν_i are the multipliers enforcing the normalization of $\pi(\cdot|i)$. Setting $\frac{\partial F'}{\partial \pi(j|i)} = 0$ yields the Gibbs distribution:

$$\pi_Y^{\beta}(j|i) = \text{softmax}_j(-\beta \, d_{\text{avg}}(x_i, y_j)) = \frac{\exp\{-\beta \, d_{\text{avg}}(x_i, y_j)\}}{\sum_{\ell=1}^K \exp\{-\beta \, d_{\text{avg}}(x_i, y_\ell)\}},$$
 (1)

where $d_{\text{avg}}(x_i, y_j) := \sum_{k=1}^K p(k|j, i) \, d(x_i, y_k)$ represents the average cost of assigning entity i to cluster j under autonomy-aware reassignments. The Gibbs distribution (1) assigns higher probability to clusters with smaller average costs. The parameter β acts as an annealing factor controlling the sharpness of assignments: when β is small, $\pi_Y^{\beta}(j|i)$ approaches a uniform distribution over clusters (high entropy), encouraging exploration; as $\beta \to \infty$, assignments become increasingly deterministic, converging toward the hard clustering of Problem (P2).

Substituting the Gibbs distribution into $(P(\beta))$ eliminates the policy variables and yields the *free* energy F as a function of the cluster representatives $Y = [y_1^\top \ y_2^\top \ \dots \ y_K^\top]^\top \in \mathbb{R}^{Kd}$:

$$\min_{Y} F(Y) = -\frac{1}{\beta} \sum_{i=1}^{N} \rho(i) \log \left(\sum_{j=1}^{K} \exp\left\{-\beta d_{\text{avg}}(x_i, y_j)\right\} \right).$$
 (\hat{P}(\beta))

The cluster representatives $\{y_\ell\}$ are obtained by minimizing $(\hat{P}(\beta))$, either by solving $\frac{\partial F}{\partial Y} = 0$ or via a descent method (Luenberger et al., 1984). For the commonly used squared Euclidean cost $d(x_i, y_k) = ||x_i - y_k||_2^2$, the optimality condition yields the update rule:

$$y_{\ell} = \frac{\sum_{i=1}^{N} \sum_{j=1}^{K} \rho(i) \, p(\ell|j, i) \, \pi_{Y}^{\beta}(j|i) \, x_{i}}{\sum_{i=1}^{N} \sum_{j=1}^{K} \rho(i) \, p(\ell|j, i) \, \pi_{Y}^{\beta}(j|i)}, \quad \forall \, 1 \le \ell \le K.$$
 (2)

Equations (1) and (2) are therefore coupled and must be solved iteratively at each β . Algorithm 1 summarizes the procedure for computing these solutions under the assumptions that the autonomy probabilities p(k|j,i) are known and independent of Y; here the cost function is squared Euclidean

Algorithm 1: Autonomy-aware clustering - when local autonomy is known explicitly

```
Input: \beta_{\min}, \beta_{\max}, \tau, K, \{x_i\}_{i=1}^N, \rho(i), and p(k|j,i) for all 1 \leq j, k \leq K and 1 \leq i \leq N;

Output: Assignment policy \pi, and cluster representatives \{y_\ell\}_{\ell=1}^K

Initialize: \beta = \beta_{\min}, \pi_Y(j|i) = \frac{1}{K} \ \forall i, j, and \{y_\ell\}_{\ell=1}^K using (2).

while \beta \leq \beta_{\max} do

while until convergence do

Compute \{\pi_Y(j|i)\} in (1), \{y_\ell\} in (2)

\beta \leftarrow \tau\beta; set y_\ell \leftarrow y_\ell + \epsilon_{\text{noise}} (to escape saddle) \forall \ell
```

(though the approach generalizes to other dissimilarity notions and cases where p(k|j,i) depends on Y). In Section (4), we develop a framework for determining clustering solutions when the local autonomy is unknown (and possibly dependent on Y) — the more common scenario in practice.

Remark. (1) reinforces that annealing promotes insensitivity to initialization: for small β , $\pi(j|i) \approx 1/K$, producing nearly uniform assignments, while increasing β gradually emphasizes the distortion term D in $(P(\beta))$, breaking uniformity. In the limit $\beta \to \infty$, π_Y^{β} collapses to hard assignments, recovering the solution of (P2). This annealing induces a homotopy from the convex surrogate -H to the original non-convex objective D, a feature of maximum-entropy methods (Rose, 1998; Xu et al., 2014) that helps avoid poor local minima (Srivastava & Salapaka, 2020; 2021).

We analyze Algorithm 1 by separating the *inner-loop* and *outer-loop* convergence. In the inner loop, the coupled equations (1) and (2) can be solved via fixed-point iterations. These iterations can be interpreted as gradient descent steps, which ensures convergence under mild conditions. We formalize this as follows:

Theorem 1 (Inner-Loop Convergence). The fixed-point iteration defined by (1) and (2) is equivalent to gradient descent iteration of the form

$$Y(t+1) = Y(t) - \frac{1}{2} \left(\hat{P}_{\pi_{\rho}}^{Y(t)} \right)^{-1} \nabla F(Y(t)), \tag{3}$$

where $\hat{P}_{\pi_{\rho}}^{Y(t)} = P_{\pi_{\rho}}^{Y(t)} \otimes \mathbb{I}_d$, \mathbb{I}_d is the $d \times d$ identity, \otimes is the Kronecker product, and $P_{\pi_{\rho}}^{Y(t)} \in \mathbb{R}^{K \times K}$ is diagonal with $[P_{\pi_{\rho}}^{Y(t)}]_{\ell\ell} = p_{\pi_{\rho}}^{Y(t)}(\ell) := \sum_{i,j} \rho(i) \, \pi_{Y(t)}(j|i) \, p(\ell|j,i)$, representing the effective mass of cluster ℓ . The iterations (3) converge to a stationary point under the following mild assumptions:

- (i) Non-degenerate clusters: There exists c>0 such that $p_{\pi_{\rho}}^{Y(t)}(\ell)\geq c$ for all ℓ ; i.e., every cluster has non-zero mass. This is trivially satisfied for π_Y^{β} in (1) at $\beta<\infty$.
- (ii) No abrupt shift in cluster mass: Let $Y_r(t+1) = Y(t) \frac{r}{2} \left(\hat{P}_{\pi_\rho}^{Y(t)}\right)^{-1} \nabla F(Y(t)), \quad r \in (0,1]$ be the relaxed updates. Then the cluster mass change is bounded: $\max_{r \in (0,1]} p_{\pi_\rho}^{Y_r(t+1)}(\ell) < 4 p_{\pi_\rho}^{Y(t)}(\ell), \ \forall \ell, i.e., no cluster's mass increases by a factor of 4 in a single update.$

If these assumptions do not hold, there exist adaptive step-sizes σ_t such that $Y(t+1) = Y(t) - \sigma_t \nabla F(Y(t))$ still converges to a stationary point.

Proof: See Appendix A for details, including a modification of Algorithm 1 with adaptive step sizes that ensures convergence to a stationary point when assumptions are violated.

For the outer-loop (β) iterations, we highlight an important feature that motivates fast (geometric) annealing schedules. At $\beta \approx 0$, the Lagrangian F is dominated by the convex term -H, and the fixed-point iterations in Algorithm 1 converge to a global minimum. As β increases, the algorithm tracks the minimizer of F(Y) until reaching a critical value $\beta_{\rm cr}$, where the fixed point ceases to be a (local) minimum. Simulations show that the cluster representatives y_ℓ change significantly at $\beta_{\rm cr}$, a phenomenon referred to as a *phase transition*, analogous to annealing processes in statistical physics. Between successive critical points, $\mathcal{Y}=\{y_\ell\}$ remains nearly constant. The following theorems quantify $\beta_{\rm cr}$ and bound the change of Y between phase transitions, enabling the design of efficient annealing schedules in Algorithm 1.

Theorem 2 (**Phase Transitions**). The critical value of the annealing parameter at which the fixed point of (1) and (2) is no longer a minimum is

$$\beta_{cr} = \frac{1}{2\lambda_{\max}\left(\left(\hat{P}_{\pi_{\rho}}^{Y}\right)^{-\frac{1}{2}}\Delta\left(\hat{P}_{\pi_{\rho}}^{Y}\right)^{-\frac{1}{2}}\right)}, \text{ where } \Delta = \sum_{i=1}^{N}\left(\sum_{j=1}^{K}P_{A}^{ij}z_{i}z_{i}^{\top}P^{ij} - \rho(i)P^{i}z_{i}z_{i}^{\top}P^{i}\right) \tag{4}$$

is a $Kd \times Kd$ matrix, $\lambda_{\max}(\cdot)$ denotes the maximum eigenvalue, $\hat{P}_{\pi_{\rho}}^{Y}$ is positive definite as defined in (3), and $P_{\pi_{\lambda}}^{ij}$, z_{i} , P^{i} are matrices determined by π_{Y} , Y, X, and $\{p(k|j,i)\}$.

Proof: See Appendix B.

Theorem 3 (Insensitivity in-between phase transitions). Let β be sufficiently far from a critical value β_{cr} . Specifically, let $\delta > 0$ satisfy $\lambda_{\min} \left(\mathbb{I}_d - 2\beta \left(P_{\pi_\rho}^Y \right)^{-1/2} \Delta \left(P_{\pi_\rho}^Y \right)^{-1/2} \right) \geq \delta$, where $\lambda_{\min}(\cdot)$ is the minimum eigenvalue. Then, the cluster representatives evolve according to $\left\| \frac{dY}{d\beta} \right\| \leq \frac{N\sqrt{K}R_\Omega}{e\beta\delta}$, where R_Ω is the diameter of the space Ω containing \mathcal{X} . In particular, the sensitivity of Y to β decays as $\mathcal{O}(1/(\beta\delta))$, becoming smaller the farther β is from β_{cr} .

Proof: See Appendix C. The above theorems are stated for the squared Euclidean cost $d(x_i, y_k) = ||x_i - y_k||_2^2$; similar results may be derived for other distance functions with suitable modifications.

Annealing Schedule in Algorithm 1: Theorems 2 and 3 show that significant changes in Y occur only at critical points $\beta_{\rm cr}$, while Y remains nearly constant between successive critical points. This motivates an annealing schedule that steps from one $\beta_{\rm cr}$ to the next. Since exact computation of $\beta_{\rm cr}$ can be expensive, a practical alternative is a geometric schedule $\beta \leftarrow \tau \beta$, $\tau > 1$, which is computationally efficient. While Theorem 3 provides a conservative bound for small β , simulations indicate that Y changes little for β far from $\beta_{\rm cr}$ (see Appendix D for details).

4 Reinforcement-based method for Autonomy-aware clustering

To account for the local autonomy when it is not known explicitly, we develop a reinforcement-based method to *learn* the assignment policy $\pi_Y^\beta(j|i)$, as well as the representative vectors $\{y_\ell\}$. Structurally, our proposed learning algorithm parallels Algorithm 1, with the key difference that in the inner while loop (executed at fixed β), explicit expressions (or updates) of $\pi_Y^\beta(j|i)$ and $\{y_\ell\}$ are replaced with their learning counterparts. We can distinguish between two learning paradigms for autonomy-aware clustering, each motivated by a different reinforcement learning framework: (C1) when $\mathcal X$ contains a tractable number of data points, $d(x_i,y_k)$ is available in closed form, and p(l|j,i) is independent of y_ℓ ; and (C2) when the dataset is large $(N\gg 1)$, $d(x_i,y_k)$ is not available in closed form, or the local autonomy depends on y_ℓ .

In (C1), we can estimate the policy π_Y^β in (1) by learning $d_{\mathrm{avg}}(x_i,y_j)$ through straightforward Q-learning—style stochastic iterative updates (Sutton & Barto, 2018), followed by stochastic gradient descent (SGD) iterations to update the cluster representatives y_ℓ ; see Appendix E for details. Here, we expound on the learning framework for the case (C2), which is more general, and subsumes (C1). In this learning framework, we learn a function approximator $d_\theta(x_i,y_j)$ to estimate the average cost $d_{\mathrm{avg}}(x_i,y_j)$. Note that here the Q-learning type tabular method to estimate $d_{\mathrm{avg}}(x_i,y_j)$ would fail to scale $(N\gg 1)$, and SGD iterations would not be possible due to either the missing closed form of $d(x_i,y_k)$, or the dependence of p(k|j,i) on $\{y_\ell\}$ (or both) — preventing the computation of stochastic gradients. We learn the parameteric function approximator $d_\theta(x_i,y_j)$ similar to several deep RL frameworks (Mnih et al., 2015). In particular, we determine θ such that it minimizes

$$L(\theta) = \mathbb{E}_{\substack{i \sim \rho, j \sim \pi_{\theta} \\ k \sim p}} \left[\left(d(x_i, y_k) - d_{\theta}(x_i, y_j) \right)^2 \right], \text{ where } \pi_{\theta}(j|i) = \frac{e^{-\beta d_{\theta}(x_i, y_j)}}{\sum_{j'=1}^{K} e^{-\beta d_{\theta}(x_i, y_{j'})}}.$$
 (5)

In practice, $L(\theta)$ is approximated using sampled mini-batches and optimized to obtain θ . We then substitute the average cost $d_{\text{avg}}(x_i, y_j)$ with its closed-form approximator $d_{\theta}(x_i, y_j)$ in F(Y) in $(\hat{P}(\beta))$, and update the representatives $\{y_{\ell}\}$ using a descent method. See Algorithm 2 for details. In Appendix F, we present the detailed description and architecture of Adaptive Distance Estimation Network (ADEN), our proposed attention-based deep neural approximator for $d_{\text{avg}}(x_i, y_j)$.

Algorithm 2: Deep autonomy-aware clustering algorithm.

```
Input: data points \mathcal{X} = \{x_i\}_{i=1}^N, number of clusters K, annealing parameters \beta_{\min}, \beta_{\max}, \tau > 1, number of samples L, number of epochs T_d, T_y, learning rates \eta_d, \eta_y, number of batches B, batch size S, Exponential Moving Average (EMA) factor \lambda \in (0,1), perturbation spread \sigma \ll 1

Output: trained \mathrm{NN}_{\theta}, optimized cluster representatives Y, and assignment policy \pi_{\theta}

Initialize: \beta \leftarrow \beta_{\min}; \theta \leftarrow \mathrm{Xavier} initialization; Y \leftarrow \frac{1}{N} \sum_i x_i + \mathcal{N}(0, \sigma^2); \bar{d}_0(i,j) = 0 \ \forall i,j

while \beta \leq \beta_{\max} do

for t = 1 to T_d do

Sample mini-batches \{\mathcal{I}_b\}_{b=1}^B, \mathcal{I}_b = \{i_q : 1 \leq q \leq S, i_q \sim \rho\}; \tilde{Y}_b \leftarrow Y + \mathcal{N}(0,\sigma^2)

forward pass \mathrm{NN}_{\theta} to obtain predicted distances \bar{D}_{\theta}(X_b, \tilde{Y}_b) for all mini-batches for each i \in \mathcal{I}_b (in parallel) do

j \sim \epsilon-greedy (\pi_{\theta}(\cdot \mid i)) with \pi_{\theta}(j \mid i) in (5)

draw \hat{L} samples k_{\ell} \sim p(k \mid j, i); compute the empirical mean \hat{d}_t(i,j) = \frac{1}{\hat{L}} \sum_{\ell=1}^{\hat{L}} d(i,k_{\ell})

update the estimate \bar{d}_t(i,j) \leftarrow \lambda \bar{d}_{t-1}(i,j) + (1-\lambda) \hat{d}_t(i,j); set \mathcal{M}_b \leftarrow \mathcal{M}_b \cup (i,j)

update \theta with one AdamW step on: L(\theta) = \frac{1}{B} \sum_{b=1}^B \sum_{(i,j) \in \mathcal{M}_b} \left[\bar{d}_t(i,j) - d_{\theta}(x_i, \tilde{y}_j)\right]^2.

for t = 1 to T_y do

Substitute d_{\mathrm{avg}}(x_i, y_j) in F(Y) in (\hat{P}(\beta)) with d_{\theta}(x_i, y_j); perform Y \leftarrow Y - \eta_y \nabla_Y F(Y)
```

5 SIMULATIONS

To evaluate how well our framework accounts for local autonomy, we test it on the synthetic dataset in Figure 1(a), designing scenarios with varying autonomy levels. In some cases, the autonomy p(k|j,i) explicitly depends on the parameters $\mathcal X$ and $\mathcal Y$; in others, it is independent. These settings capture realistic behaviors where an entity i may reject its prescribed cluster j and instead join another $k \neq j$. Here we choose the local autonomy model such that, with probability $1-\kappa$, the entity i accepts its prescribed cluster j; otherwise, with probability κ , it chooses an alternative cluster $k \neq j$ according to a softmax distribution, $p(k|j,i) = \kappa \frac{\exp[-c_k(j,i)/T]}{\sum_{t\neq j} \exp[-c_t(j,i)/T]}$, where the cost $c_k(j,i) = \zeta d(y_j,y_k) + \gamma d(x_i,y_k)$ balances cluster-cluster distance (ζ) and cluster-entity distance (γ). Here, κ controls override frequency, and T regulates randomness (uniform as $T \to \infty$, deterministic as $T \to 0$). Varying $\{\kappa, T, \zeta, \gamma\}$ yields diverse autonomy scenarios that affect both cluster locations $\{y_\ell\}$ and the central-planner policy π_Y^β . Full hyperparameters of ADEN in different scenarios appear in Appendix G.

We compare Algorithm 1 (ground truth), Algorithm 2 (ADEN-based), and a baseline that ignores autonomy. Table 1 reports objective gaps relative to ground truth, for the dataset in figure 1. The ADEN-based algorithm incurs only modest error: median 3.12%, mean 3.42%, with deviations from 1.40% (small κ) to 8.03% (intermediate κ). By contrast, ignoring autonomy produces severe degradation: median 30.84%, mean 36.26%, and up to 100.20%. Performance in this baseline worsens as κ increases, while the performance of the ADEN-based algorithm is independent of it and can be further improved through hyperparameter tuning, underscoring its robustness across varying autonomy levels.

As a second illustrative example, we consider *decentralized sensing* in urban traffic monitoring. Using the UDT19 London Traffic dataset (Loder et al., 2019), which provides geocoordinates of road-side traffic sensors across Greater London, we pose a *facility-location* problem: determine optimal UAV positions to maximize coverage of the sensor network. In practice, sensors may occasionally fail to transmit data to their assigned UAV due to network uncertainties such as packet loss or congestion (Psannis, 2016). When this occurs, a sensor forwards its measurements to a different UAV, with higher probability for UAVs in adjacent clusters—naturally introducing local autonomy.

We model this behavior using the same transition distribution p(k|j,i) described earlier, setting $\gamma=0, \ \zeta=1$, and varying $\kappa\in\{0.1,0.5\}$ and $T\in\{0.1,0.01\}$. The temperature T controls the sharpness of the softmax: lower values create a strong preference for selecting nearby UAVs whenever the assigned policy cannot be satisfied, while the two κ values represent low and high rates of network faults. Figure 2 reports the solutions obtained by ADEN (Algorithm 2).

Table 1: D gap (%) of the ADEN versus the setting that ignores local autonomy p(k|j,i), relative to the ground truth (Algorithm 1) across scenarios where p(k|j,i) depends on Y.

κ	γ	ζ	T	ADEN	Ignored
0.1	0	1	0.01	2.11	10.73
0.1	0	1	100	2.08	6.67
0.1	0.5	1	0.01	1.87	10.01
0.2	0	1	0.01	3.01	25.80
0.2	0	1	100	1.79	15.08
0.2	0.5	1	0.01	1.50	24.90
0.2	0.5	1	100	1.40	15.06
0.3	0	1	0.01	4.80	44.62
0.3	0	1	100	3.25	24.71

κ	γ	ζ	T	ADEN	Ignored
0.3	0.5	1	0.01	7.02	43.56
0.3	0.5	1	100	3.24	24.69
0.4	0	1	0.01	8.03	68.89
0.4	0	1	100	3.36	35.92
0.4	0.5	1	0.01	3.47	67.63
0.4	0.5	1	100	2.68	35.89
0.5	0	1	100	5.66	49.21
0.5	0.5	1	0.01	1.72	100.20
0.5	0.5	1	100	4.66	49.17

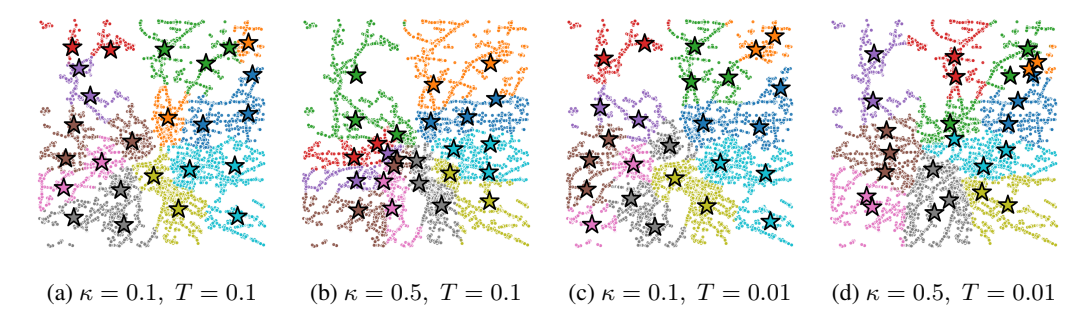


Figure 2: Clustering of the UDT19 dataset under parameterized autonomy for varying κ . UAVs are indicated by colored stars, and sensor (denoted by *) colors denote their associated UAV.

The results demonstrate a consistent pattern. Increasing κ causes the UAV (cluster) representatives to move closer together (closer to the centroid of the entire dataset), reflecting stronger cross-cluster autonomy ((Figure 2(b),2(d))). Whereas, in case of low κ , the UAVs are fairly spread out (Figure 2(a),2(c)). This intuitive outcome is accurately captured by our learned model (ADEN) in both temperature regimes.

Notably, when $\kappa=0.1, T=0.1$, ADEN matches the performance of the model-based baseline (ground truth), and for $\kappa=0.5, T=0.1$ it achieves approximately a 10% improvement over the ground truth, despite the absence of an explicit autonomy model. These results underscore the ability of our approach to remain competitive with, and in some cases surpass, model-aware methods while scaling to large, high-dimensional decentralized sensing problems.

The case T=0.01 is particularly challenging: the distribution p(k|j,i) becomes sharply peaked, and the large number of entities and clusters add to this challenge. Even in this setting, our model-free solution attains average optimality gaps of only 18.37% and 24.82% for $\kappa=0.1$ and $\kappa=0.5$, respectively, relative to a model-based oracle. These gaps can be further reduced through standard hyperparameter tuning and extended training. Finally, we emphasize that Algorithm 2, being rooted in a reinforcement learning framework, can be naturally deployed in an online setting where it continuously learns and refines the solution.

REPRODUCIBILITY STATEMENT

- 1. For all the theorems presented in this work, the complete details of the underlying assumptions (if any) and the full proofs are provided in the Appendix, with appropriate references made in the main text.
- 2. The codes were executed on a GPU Cluster, specifically utilizing the ghx4 partition. This system is comprised of NVIDIA Grace Hopper Superchip nodes, each equipped with an NVIDIA H100 GPU and a Grace CPU. The node provided 16 CPU cores and 1 GPU, with a total of 64 GB of memory allocated for the job.

- 3. The random seeds / hyperparameter settings for all the simulations in Section 5 are provided in the Appendix G.
- 4. For the simulations reported in Section 5, the corresponding datasets and implementation codes are included in the supplementary material. Also, the code and data will be made publicly available on Github once review is completed.
- 5. Similarly, for the simulations described in Appendix D, the relevant dataset (data point locations and their autonomy levels) is also included in the same supplementary material. The code to reproduce the plots here are straightforward and based on Algorithm 1. The inputs involved are $\beta_{\min} = 10^{-3}$, $\beta_{\max} = 10^3$, $\tau = 0.99$, $\rho(i) = \frac{1}{N}$, $\epsilon_{\text{noise}} \sim (10^{-4})\mathcal{N}(0,1)$.

REFERENCES

- Sanchayan Banerjee and Giuseppe A Veltri. Harnessing pluralism in behavioral public policy requires insights from computational social science. *Frontiers in Behavioral Economics*, 3:1503793, 2024.
- Salar Basiri, Alisina Bayati, and Srinivasa Salapaka. Orthogonal nonnegative matrix factorization with sparsity constraints, 2025. URL https://arxiv.org/abs/2210.02672.
- Vivek S Borkar and Vivek S Borkar. Stochastic approximation: a dynamical systems viewpoint, volume 100. Springer, 2008.
- Brian Brubach, Nathaniel Grammel, David G. Harris, Aravind Srinivasan, Leonidas Tsepenekas, and Anil Vullikanti. Stochastic optimization and learning for two-stage supplier problems. *ACM Trans. Probab. Mach. Learn.*, 1(1), December 2024. doi: 10.1145/3604619. URL https://doi.org/10.1145/3604619.
- Hongbo Deng and Jiawei Han. Probabilistic models for clustering. In *Data Clustering*, pp. 61–86. Chapman and Hall/CRC, 2018.
- Mario A. T. Figueiredo and Anil K. Jain. Unsupervised learning of finite mixture models. *IEEE Transactions on pattern analysis and machine intelligence*, 24(3):381–396, 2002.
- Shreyank N Gowda, Laura Sevilla-Lara, Frank Keller, and Marcus Rohrbach. Claster: clustering with reinforcement learning for zero-shot action recognition. In *European conference on computer vision*, pp. 187–203. Springer, 2022.
- David G Harris, Shi Li, Thomas Pensyl, Aravind Srinivasan, and Khoa Trinh. Approximation algorithms for stochastic clustering. *Journal of Machine Learning Research*, 20(153):1–33, 2019.
- Thomas Hofmann. Probabilistic latent semantic analysis. arXiv preprint arXiv:1301.6705, 2013.
- Jiaming Ji, Tianyi Qiu, Boyuan Chen, Borong Zhang, Hantao Lou, Kaile Wang, Yawen Duan, Zhonghao He, Jiayi Zhou, Zhaowei Zhang, et al. Ai alignment: A comprehensive survey. *arXiv* preprint arXiv:2310.19852, 2023.
- Md Rezaul Karim, Oya Beyan, Achille Zappa, Ivan G Costa, Dietrich Rebholz-Schuhmann, Michael Cochez, and Stefan Decker. Deep learning-based clustering approaches for bioinformatics. *Briefings in bioinformatics*, 22(1):393–415, 2021.
- Michael Kearns and Aaron Roth. *The Ethical Algorithm: The Science of Socially Aware Algorithm Design*. Oxford University Press, Inc., USA, 2019. ISBN 0190948205.
- Peng Li, Jing Gao, Jianing Zhang, Shan Jin, and Zhikui Chen. Deep reinforcement clustering. *IEEE Transactions on Multimedia*, 25:8183–8193, 2022.
- Aristidis Likas. A reinforcement learning approach to online clustering. *Neural computation*, 11(8): 1915–1932, 1999.
 - Allister Loder, Lukas Ambühl, Monica Menendez, and Kay W Axhausen. Understanding traffic capacity of urban networks. *Sci. Rep.*, 9(1):16283, November 2019.

- David G Luenberger, Yinyu Ye, et al. *Linear and nonlinear programming*, volume 2. Springer, 1984
- Christos N Mavridis and John S Baras. Online deterministic annealing for classification and clustering. *IEEE Transactions on Neural Networks and Learning Systems*, 34(10):7125–7134, 2022.
 - Geoffrey J McLachlan and Kaye E Basford. Mixture models. inference and applications to clustering. *Statistics: textbooks and monographs*, 1988.
 - Geoffrey J McLachlan and Thriyambakam Krishnan. *The EM algorithm and extensions*. John Wiley & Sons, 2008.
 - Geoffrey J McLachlan and David Peel. Finite mixture models. John Wiley & Sons, 2000.
 - Volodymyr Mnih, Koray Kavukcuoglu, David Silver, Andrei A Rusu, Joel Veness, Marc G Bellemare, Alex Graves, Martin Riedmiller, Andreas K Fidjeland, Georg Ostrovski, et al. Human-level control through deep reinforcement learning. *Nature*, 518(7540):529–533, 2015.
 - Maryam Negahbani and Deeparnab Chakrabarty. Better algorithms for individually fair k-clustering. In M. Ranzato, A. Beygelzimer, Y. Dauphin, P.S. Liang, and J. Wortman Vaughan (eds.), Advances in Neural Information Processing Systems, volume 34, pp. 13340–13351. Curran Associates, Inc., 2021. URL https://proceedings.neurips.cc/paper_files/paper/2021/file/6f221fcb5c504fe96789df252123770b-Paper.pdf.
 - Kostas E Psannis. Hevc in wireless environments. *Journal of Real-Time Image Processing*, 12(2): 509–516, 2016.
 - Kenneth Rose. *Deterministic annealing, clustering, and optimization*. PhD thesis, California Institute of Technology, 1991.
 - Kenneth Rose. Deterministic annealing for clustering, compression, classification, regression, and related optimization problems. *Proceedings of the IEEE*, 86(11):2210–2239, 1998.
 - Cristian Rusu, John Thompson, and Neil M. Robertson. Sensor scheduling with time, energy, and communication constraints. *IEEE Transactions on Signal Processing*, 66(2):528–539, 2018. doi: 10.1109/TSP.2017.2773429.
 - Jaswinder Singh and Damanpreet Singh. A comprehensive review of clustering techniques in artificial intelligence for knowledge discovery: Taxonomy, challenges, applications and future prospects. *Advanced Engineering Informatics*, 62:102799, 2024. ISSN 1474-0346. doi: https://doi.org/10.1016/j.aei.2024.102799. URL https://www.sciencedirect.com/science/article/pii/S1474034624004476.
 - Amber Srivastava and Srinivasa M Salapaka. Simultaneous facility location and path optimization in static and dynamic networks. *IEEE Transactions on Control of Network Systems*, pp. 1–1, 2020.
 - Amber Srivastava and Srinivasa M Salapaka. Parameterized mdps and reinforcement learning problems—a maximum entropy principle-based framework. *IEEE Transactions on Cybernetics*, 52 (9):9339–9351, 2021.
 - Richard S Sutton and Andrew G Barto. Reinforcement learning: An introduction. MIT press, 2018.
 - Ashish Vaswani, Noam Shazeer, Niki Parmar, Jakob Uszkoreit, Llion Jones, Aidan N Gomez, Łukasz Kaiser, and Illia Polosukhin. Attention is all you need. *Advances in neural information processing systems*, 30, 2017.
 - Yunwen Xu, Srinivasa M Salapaka, and Carolyn L Beck. Aggregation of graph models and markov chains by deterministic annealing. *IEEE Transactions on Automatic Control*, 59(10):2807–2812, 2014.
 - Saneh Lata Yadav and RL Ujjwal. Mitigating congestion in wireless sensor networks through clustering and queue assistance: a survey. *Journal of Intelligent Manufacturing*, 32(8):2083–2098, 2021.

Yi Zhang, Miaomiao Li, Siwei Wang, Sisi Dai, Lei Luo, En Zhu, Huiying Xu, Xinzhong Zhu, Chaoyun Yao, and Haoran Zhou. Gaussian mixture model clustering with incomplete data. *ACM Trans. Multimedia Comput. Commun. Appl.*, 17(1s), March 2021. ISSN 1551-6857. doi: 10. 1145/3408318. URL https://doi.org/10.1145/3408318.

Jiawei Zhu, Xuegang Wu, and Liu Yang. Edge-constraint based multi-scale contrastive learning for image deep clustering. *Digital Signal Processing*, 163:105180, 2025. ISSN 1051-2004. doi: https://doi.org/10.1016/j.dsp.2025.105180. URL https://www.sciencedirect.com/science/article/pii/S1051200425002027.

A CONVERGENCE PROOF

A.1 CASE A: WHEN THE ASSUMPTIONS IN THEOREM 1 HOLD TRUE

Parts of the proof below require hessian of F(Y) in $(\hat{P}(\beta))$, which is computed in the Appendix B. We refer to the relevant equations from Appendix B wherever required.

We have the following assumptions:

- (i) Non-degenerate clusters there exists c>0 such that $p_{\pi_\rho}^{Y(t)}(l)\geq c$ for all l. In other words, each cluster is a of non-zero mass. Note that this is trivially true for π_Y^β in (1) at $\beta<\infty$.
- (ii) No abrupt shift in cluster mass let $Y_r(t+1) = Y(t) \frac{r}{2} \left(\hat{P}_{\pi_\rho}^{Y(t)}\right)^{-1} \nabla F(Y(t))$ be the relaxed update of the iteration in (3), where $r \in (0,1]$. Then the change in cluster mass from t and t+1 is upper bounded. In particular, $\max_{r \in (0,1]} p_{\pi_\rho}^{Y_r(t+1)}(\ell) < 4p_{\pi_\rho}^{Y(t)}(\ell)$ for all ℓ , i.e., the ℓ^{th} cluster mass at t+1 does not increase by more than 4 times of that at t for all possible values of $r \in (0,1]$.

Consider fixed point iterations in the inner-loop of the Algorithm 1. Substituting the policy $\pi_Y^{\beta}(j|i)$ in (1) into the expression for the representative features y_{ℓ} in (2) results into

$$y_{\ell} = \frac{\sum_{i=1}^{N} \sum_{j=1}^{K} \rho(i) p(l|j, i) \frac{\exp\{-\beta d_{\text{avg}}(x_{i}, y_{j})\}}{\sum_{j'=1}^{K} \exp\{-\beta d_{\text{avg}}(x_{i}, y_{j'})\}} x_{i}}{\sum_{i=1}^{N} \sum_{j=1}^{K} \rho(i) p(l|j, i) \frac{\exp\{-\beta d_{\text{avg}}(x_{i}, y_{j})\}}{\sum_{i'=1}^{K} \exp\{-\beta d_{\text{avg}}(x_{i}, y_{j'})\}}}.$$
(6)

Thus, one pass over the equations in (1) and (2) is analogous to the iteration

$$y_{\ell}(t+1) = \frac{\sum_{i=1}^{N} \sum_{j=1}^{K} \rho(i) p(l|j, i) \frac{\exp\{-\beta d_{\text{avg}}(x_{i}, y_{j}(t))\}}{\sum_{j'=1}^{K} \exp\{-\beta d_{\text{avg}}(x_{i}, y_{j'}(t))\}} x_{i}}{\sum_{i=1}^{N} \sum_{j=1}^{K} \rho(i) p(l|j, i) \frac{\exp\{-\beta d_{\text{avg}}(x_{i}, y_{j}(t))\}}{\sum_{j'=1}^{K} \exp\{-\beta d_{\text{avg}}(x_{i}, y_{j'}(t))\}}} \, \forall \, l,$$
 (7)

$$\Rightarrow y_{\ell}(t+1)p_{\pi_{\rho}}^{Y(t)}(l) = \sum_{i=1}^{N} \sum_{j=1}^{K} \rho(i)p(l|j,i)\pi_{Y(t)}^{\beta}(j|i)x_{i}, \text{ where}$$
(8)

$$\pi_{Y(t)}^{\beta}(j|i) = \frac{\exp\{-\beta d_{\text{avg}}(x_i, y_j(t))\}}{\sum_{j'=1}^{K} \exp\{-\beta d_{\text{avg}}(x_i, y_{j'}(t))\}} \text{ and } p_{\pi_{\rho}}^{Y(t)}(l) = \sum_{i=1}^{N} \rho(i) \sum_{j=1}^{K} p(l|j, i) \pi_{Y(t)}^{\beta}(j|i). \text{ Substituted in the property of the property$$

tracting $p_{\pi_{\rho}}^{Y(t)}(l)y_{\ell}(t)$ from both sides of the equation (8), we obtain

$$(y_{\ell}(t+1) - y_{\ell}(t)) p_{\pi_{\rho}}^{Y(t)}(l) = -\sum_{i=1}^{N} \sum_{j=1}^{K} \rho(i) p(l|j, i) \pi_{Y(t)}^{\beta}(j|i) (y_{\ell}(t) - x_i)$$
 (9)

$$\Rightarrow \left(y_{\ell}(t+1) - y_{\ell}(t)\right) p_{\pi_{\rho}}^{Y(t)}(l) = -\frac{\partial F(Y(t))}{\partial y_{\ell}},\tag{10}$$

which in the stacked vector notation can be re-written as

$$Y(t+1) = Y(t) - \frac{1}{2} (\hat{P}_{\pi_{\rho}}^{Y(t)})^{-1} \nabla F(Y(t)) =: Y(t) + S(t).$$
(11)

Here, $\hat{P}_{\pi_{\rho}}^{Y(t)} = P_{\pi_{\rho}}^{Y}(t) \otimes I_{d}$, I_{d} is a $d \times d$ Identity matrix, \otimes denotes the Kronecker product, $P_{\pi_{\rho}}^{Y(t)} \in \mathbb{R}^{K \times K}$ is a positive definite diagonal matrix with $\left[P_{\pi_{\rho}}^{Y(t)}\right]_{ll} = p_{\pi_{\rho}}^{Y(t)}(l) \geq c > 0$, $\nabla F(Y(t)) = \left[\frac{dF(Y(t))}{dy_{1}}^{\top}, \cdots, \frac{dF(Y(t))}{dy_{K}}^{\top}\right]^{\top} \in \mathbb{R}^{Kd}$. At every time instant t, we define

$$L(Y(t)) := \sup_{r \in [0,1]} \lambda_{\max} \left(\left(\hat{P}_{\pi_{\rho}}^{Y(t)} \right)^{-1/2} \nabla^{2} F(Y(t) + rS(t)) \left(P_{\pi_{\rho}}^{Y(t)} \right)^{-1/2} \right), \tag{12}$$

Let $Y_r(t+1) := Y(t) + rS(t)$, and $g(r) := F(Y_r(t+1))$. Then $g'(r) = \nabla F(Y_r(t+1))^{\top}S(t)$, $g''(r) = S(t)^{\top}\nabla^2 F(Y_r(t+1))^{\top}S(t)$. To avoid notational clutter, let $M_t := (\hat{P}_{\pi_\rho}^{Y(t)})^{-1/2}\nabla^2 F(Y_r(t+1))(P_{\pi_\rho}^{Y(t)})^{-1/2}$. Then

$$g''(r) = \left(\left(\hat{P}_{\pi_{\rho}}^{Y(t)} \right)^{1/2} S(t) \right)^{\top} M_t \left(\left(\hat{P}_{\pi_{\rho}}^{Y(t)} \right)^{1/2} S(t) \right)$$
 (13)

$$\Rightarrow g''(r) \le \lambda_{\max}(M_t) \left(S(t)^{\top} \left(\hat{P}_{\pi_o}^{Y(t)} \right) S(t) \right)$$
(14)

$$\Rightarrow g''(r) \le \lambda_{\max}(M_t) \|S\|_{P_{\pi_o}^{Y(t)}}^2 \le L(Y(t)) \|S(t)\|_{P_{\pi_o}^{Y(t)}}^2 \tag{15}$$

Integrating both sides we obtain

$$g(1) = g(0) + g'(0) + \int_0^1 (1 - t)g''(t)dt$$
(16)

$$\Rightarrow F(Y(t+1)) \le F(Y(t)) + \nabla F(Y(t))^{\top} S(t) + L(Y(t)) \|S(t)\|_{P_{\pi_{\rho}}^{Y(t)}}^{2} \int_{0}^{1} (1-t)dt \tag{17}$$

$$\Rightarrow F(Y(t+1)) \le F(Y(t)) + \nabla F(Y(t))^{\top} S(t) + \frac{1}{2} L(Y(t)) ||S||_{P_{\pi_{\rho}}^{Y(t)}}^{2}$$
(18)

Substituting $S(t) = -\frac{1}{2} \left(\hat{P}_{\pi_{\rho}}^{Y(t)} \right)^{-1} \nabla F(Y(t))$ in (18), we get:

$$F(Y(t+1)) \le F(Y(t)) - \frac{1}{2} \nabla F(Y(t))^{\top} \left(P_{\pi_{\rho}}^{Y(t)} \right)^{-1} \nabla F(Y(t)) + \frac{1}{8} L(Y(t)) \left(\nabla F(Y(t))^{\top} \left(P_{\pi_{\rho}}^{Y(t)} \right)^{-1} \right) \nabla F(Y(t)) \right)$$
(19)

$$\Rightarrow \left(\frac{1}{2} - \frac{1}{8}L(Y(t))\right) \|\nabla F(Y(t))\|_{\left(P_{\pi_{o}}^{Y(t)}\right)^{-1}} \le F(Y(t)) - F(Y(t+1)) \tag{20}$$

Telescopic summation over all $t \in \{0, 1, ..., T\}$ gives us

$$\sum_{t=0}^{T} \nu_{t} \|\nabla F(Y(t))\|_{\left(P_{\pi_{\rho}}^{Y(t)}\right)^{-1}} \le F(Y(0)) - F(Y(T)), \text{ where } \nu_{t} = \frac{1}{2} - \frac{1}{8}L(Y(t))$$
 (21)

$$\Rightarrow \sum_{t=0}^{T} \nu_t \|\nabla F(Y(t))\|_{\left(P_{\pi_\rho}^{Y(t)}\right)^{-1}} \le F(Y(0)) - F_{\min} < \infty \tag{22}$$

There always exists a minimum F_{\min} such that $F(Y(T)) \geq F_{\min}$ for all Y; note that for $0 < \beta < \infty$, the Log-Sum-Exponential function F(Y(T)) in $(\hat{\mathbf{P}}(\beta))$ is always lower bounded. Thus, if $\nu_t > 0 \forall t$, then, as $T \to \infty$, $\|\nabla F(Y(T))\|_{\left(P_{\pi^o}^{Y(T)}\right)^{-1}} \to 0$.

The condition $\nu_t > 0$ holds true if L(Y(t)) < 4. We have from (49) in Appendix B that

$$\nabla^{2} F(Y_{r}(t+1)) = \hat{P}_{\pi_{\rho}}^{Y_{r}(t+1)} - 2\beta \underbrace{\sum_{i=1}^{N} \left(\sum_{j=1}^{K} P_{A}^{ij} z_{i} z_{i}^{\top} P^{ij} - \rho(i) P^{i} z_{i} z_{i}^{\top} P^{i} \right)}_{-\Delta}, \tag{23}$$

where $\hat{P}_{\pi_{\rho}}^{Y_r(t+1)}$ is positive definite by definition in Appendix B, and the matrix Δ is positive semi-definite too under the definition of the matrices P_A^{ij}, z, P^{ij}, P^i detailed in Appendix B. Actually, the latter follows from the fact that for any $\Psi = [\psi_1^\top \dots \psi_K^\top]^\top \in \mathbb{R}^{Kd}, \Psi^\top \Delta \Psi = \sum_{i=1}^N \rho(i)\delta_i$, where

$$\delta_i = \sum_{j=1}^K \pi_Y^{\beta}(j|i) \left(\sum_{k=1}^K p(k|j,i) [y_k - x_i]^\top \psi_k \right)^2 - \left(\sum_{j,k=1}^K \pi_Y^{\beta}(j|i) p(k|j,i) [y_k - x_i]^\top \psi_k \right)^2. \tag{24}$$

Note that $\delta_i \geq 0$, because variance of $\left(\sum_{k=1}^K p(k|j,i)[y_k-x_i]^\top \psi_k\right)$ computed with respect to the distribution $\pi_Y^\beta(\cdot|i)$ is always non-negative. Thus, we can say that $\nabla^2 F(Y_r(t+1)) \preceq P_{\pi_\rho}^{Y_r(t+1)}$, in other words $P_{\pi_\rho}^{Y_r(t+1)} - \nabla^2 F(Y_r(t+1))$ is positive semi-definite. Thus, we have that

$$\lambda_{\max} \left(\left(\hat{P}_{\pi_{\rho}}^{Y(t)} \right)^{-1/2} \nabla^{2} F(Y_{r}(t+1)) \left(P_{\pi_{\rho}}^{Y(t)} \right)^{-1/2} \right) \leq \lambda_{\max} \left(\left(\hat{P}_{\pi_{\rho}}^{Y(t)} \right)^{-1} \hat{P}_{\pi_{\rho}}^{Y_{r}(t+1)} \right) \tag{25}$$

$$\Rightarrow L(Y(t)) \le \max_{r \in [0,1]} \lambda_{\max} \left(\left(\hat{P}_{\pi_{\rho}}^{Y(t)} \right)^{-1} \hat{P}_{\pi_{\rho}}^{Y_{r}(t+1)} \right) = \max_{r \in [0,1]} \max_{1 \le l \le K} \frac{p_{\pi_{\rho}}^{Y_{r}(t+1)}(l)}{p_{\pi_{\rho}}^{Y(t)}(l)}. \tag{26}$$

Under the assumption that for any cluster, its mass does not drastically change, i.e., $\frac{p_{\pi\rho}^{Y_r(t+1)}}{p_{\pi\rho}^{Y(t)}} < 4$ for all $r \in (0,1]$, we obtain that L(Y(t)) < 4. Thus $\nu_t > 0$, and $\|\nabla F(Y(T))\|_{\left(P_{\pi\rho}^{Y(T)}\right)^{-1}} \to 0$ as $T \to \infty$. This is equivalent to $\nabla F(Y(T)) \to 0$, which implies that the iterations (11) converge to a stationary point.

A.2 CASE B: WHEN THE ASSUMPTIONS IN THEOREM 1 DO NOT HOLD

Here, we replace the gradient descent steps in (3) with descent steps of the form

$$Y(t+1) = Y(t) - \sigma_t \nabla F(Y(t)) =: Y(t) + \sigma_t S(t), \tag{27}$$

where the step-size σ_t is designed using Armijo's rule (Luenberger et al., 1984). More precisely, we follow the following steps:

- 1. Let $m=0, \sigma_{m,t}=s, \rho\in(0,1), \xi\in(0,1)$ be Armijo's parameter.
- 2. Check if

$$F(Y(t) - \sigma_{m,t} \nabla F(Y(t))) - F(Y(t)) \le -\varrho \sigma_{m,t} \|\nabla F(Y(t))\|_2^2$$
(28)

3. If yes: $\sigma_t \leftarrow \sigma_{m,t}$ and exit. If not: $\sigma_{m+1,t} = \xi \sigma_{m,t}$, $m \leftarrow m+1$. Go to step 2.

Note that if the above steps terminate, then we obtain a step size σ_t that enables descent $F(Y(t) - \sigma_t \nabla F(Y(t))) \leq F(Y(t))$. We next show that for the free-energy function F(Y) in $(\hat{\mathbf{P}}(\beta))$ the above steps always converge. In other words, we show that there always exists a σ_t such that $F(Y(t) - \sigma_t \nabla F(Y(t))) \leq F(Y(t))$.

$$L_{\sigma}(Y(t)) := \sup_{r \in [0,1]} \lambda_{\max} \Big(\nabla^2 F(Y(t) + r\sigma_t S(t)) \Big)$$
(29)

Let $Y_{r,\sigma}^t = Y(t) + r\sigma_t S(t)$, $h(r) := F(Y_{r,\sigma}^t)$. Then, $h'(r) = \sigma_t \nabla F(Y_{r,\sigma}^t)^\top S(t)$, $h''(r) = \sigma_t^2 S(t)^\top \nabla^2 F(Y_{r,\sigma}^t) S(t)$. To avoid notational clutter, let $\hat{M}_t := \nabla^2 F(Y(t) + r\sigma_t S(t))$. Then

$$h''(r) = \sigma_t^2 (S(t))^\top \hat{M}_t (S(t))$$
(30)

$$\Rightarrow h''(r) \le \sigma_t^2 \lambda_{\max}(\hat{M}_t) \Big(S(t)^\top S(t) \Big)$$
(31)

$$\Rightarrow h''(r) \le \sigma_t^2 \lambda_{\max}(\hat{M}_t) \|S(t)\|_2^2 \le \sigma_t^2 L_{\sigma}(Y(t)) \|S(t)\|_2^2$$
(32)

Integrating both sides we obtain

$$h(1) = h(0) + h'(0) + \int_0^1 (1 - t)h''(t)dt$$
(33)

$$\Rightarrow F(Y(t) + \sigma_t S(t)) \le F(Y(t)) + \sigma_t \nabla F(Y(t))^{\top} S(t) + \sigma_t^2 \frac{1}{2} L_{\sigma}(Y(t)) \|S(t)\|_2^2$$
 (34)

Setting step-size at $\sigma_{m,t}$ in (34), we obtain

$$F(Y(t) - \sigma_{m,t} \nabla F(Y(t))) - F(Y(t)) \le \sigma_{m,t} \nabla F(Y(t))^{\top} S(t) + \frac{\sigma_{m,t}^2}{2} L_{\sigma}(Y(t)) \|S(t)\|_2^2$$
 (35)

The Armijo's condition in (28) will be true if

$$\sigma_{m,t} \nabla F(Y(t))^{\top} S(t) + \frac{\sigma_{m,t}^2}{2} L_{\sigma}(Y(t)) \|S(t)\|_2^2 \le -\varrho \sigma_{m,t} \|\nabla F(Y(t))\|_2^2$$
 (36)

Substituting $S(t) = -\nabla F(Y(t))$, we obtain

$$-\|\nabla F(Y(t))\|_{2}^{2} + \frac{\sigma_{m,t}}{2} L_{\sigma}(Y(t))\|\nabla F(Y(t))\|_{2}^{2} \le -\varrho\|\nabla F(Y(t))\|_{2}^{2}$$
(37)

 $\beta \leftarrow \tau \beta$; set $y_{\ell} \leftarrow y_{\ell} + \epsilon_{\text{noise}}$ (to escape saddle) $\forall \ell$

Algorithm 3: Autonomy-aware clustering — when assumptions in Theorem 1 fail Input: β_{\min} , β_{\max} , τ , K, \mathcal{X} , $\rho(i)$, $p(k|j,i) \, \forall \, i,j,k$, and Armijo's parameters $s,\varrho\in(0,1)$, $\xi\in(0,1)$; Output: Assignment policy π , and cluster representatives $\{y_\ell\}_{\ell=1}^K$ Initialize: $\beta=\beta_{\min}$, $\pi_Y^\beta(j|i)=\frac{1}{K} \, \forall \, i,j$, and $\{y_\ell\}_{\ell=1}^K$ using (2). while $\beta\leq\beta_{\max}$ do while until convergence do $\begin{array}{c|c} m=0; \sigma_{m,t}=s; \text{ while } True \text{ do} \\ \text{if } F(Y(t)-\sigma_{m,t}\nabla F(Y(t)))-F(Y(t))\leq -\varrho\sigma_{m,t}\|\nabla F(Y(t))\|_2^2 \text{ then} \\ \perp \sigma_t\leftarrow\sigma_{m,t}; \text{ break}; \\ \text{else} \\ \perp \sigma_{m+1,t}\leftarrow\xi\sigma_{m,t}; \quad m\leftarrow m+1 \\ Y(t+1)\leftarrow Y(t)-\sigma_t\nabla F(Y(t)); t\leftarrow t+1; \end{array}$

$$\Rightarrow -1 + \frac{\sigma_{m,t}}{2} L_{\sigma}(Y(t)) \le -\varrho \qquad \Rightarrow \sigma_{m,t} \le \frac{2}{L_{\sigma}(Y(t))} (1 - \varrho)$$
 (38)

$$\Rightarrow \sigma_{0,t}\xi^m \le \frac{2}{L_{\sigma}(Y(t))} (1 - \varrho) \tag{39}$$

Since $\xi < 1$, there exist a finite number of iterations m beyond which the above inequality will be true. In other words, Armijo's condition in (28) will be satisfied. Thus, resulting into an appropriate step size σ_t . See Algorithm 3 for details.

B PHASE TRANSITION AND CRITICAL ANNEALING PARAMETER

B.1 Hessian Computation

We define the following matrices:

- 1. $\hat{P}^{ij} \in \mathbb{R}^{K \times K}$ is a diagonal matrix, such that $[\hat{P}^{ij}]_{kk} = p(k|j,i), P^{ij} = \hat{P}^{ij} \otimes \mathbb{I}_d$, where \mathbb{I}_d is a $d \times d$ identity matrix,
- 2. $P^{i} = \sum_{j=1}^{K} \pi_{Y}^{\beta}(j|i)P^{ij}$,
- 3. $z_i = Y X^i \in \mathbb{R}^{Kd}$, where $Y = \begin{bmatrix} y_1^\top & y_2^\top & \dots & y_K^\top \end{bmatrix}^\top$, $X^i = \mathbf{1}_{Kd} \otimes x_i$, and \otimes denotes the Kronecker product.
- 4. $\hat{P}_A^{ij} \in \mathbb{R}^{K \times K}$ is a diagonal matrix; $\left[\hat{P}_A^{ij}\right]_{kk} = \rho(i)\pi_Y^{\beta}(j|i)p(k|j,i), P_A^{ij} = \hat{P}_A^{ij} \otimes \mathbb{I}_d \in \mathbb{R}^{Kd \times Kd}$
- 5. $P_{\pi_{\rho}}^{Y} \in \mathbb{R}^{K \times K}$ is a diagonal matrix such that $\left[P_{\pi_{\rho}}^{Y}\right]_{kk} = \sum_{i=1}^{N} \sum_{j=1}^{K} \rho(i) \pi_{Y}^{\beta}(j|i) p(k|j,i)$, and $\hat{P}_{\pi_{\rho}}^{Y} = P_{\pi_{\rho}}^{Y} \otimes \mathbb{I}_{d} \in \mathbb{R}^{Kd \times Kd}$. Note that, under the Gibbs' distribution of π_{Y} in (1), $\left[P_{\pi_{\rho}}^{Y}\right]_{kk} > 0$ for $\beta < \infty$, thus making $\hat{P}_{\pi_{\rho}}^{Y}$ and $P_{\pi_{\rho}}^{Y}$ positive definite matrices.

Phase transitions occur when the cluster representatives $\{y_\ell\}$ in (2), given by $\frac{\partial F}{\partial y_\ell}=0$, are no longer the local minima. In other words, $\frac{\partial F(Y)}{\partial Y}=0$, where $Y=[y_1^\top,\ldots,y_K^\top]^\top$ but, there exist some perturbation direction $\Psi=[\psi_1^\top,\ldots,\psi_K^\top]^\top\in\mathbb{R}^{Kd}$ such that the Hessian $\mathcal{H}(Y,\pi,\Psi,\beta)=$

$$\left. \frac{d^2 F(Y + \epsilon \Psi)}{d\epsilon^2} \right|_{\epsilon = 0} = \Psi^\top \left[\hat{P}_{\pi_\rho}^Y - 2\beta \left(\sum_{i=1}^N \sum_{j=1}^K P_A^{ij} z_i z_i^\top P^{ij} - \sum_{i=1}^N \rho(i) P^i z_i z_i^\top P^i \right) \right] \Psi, \quad (40)$$

is no longer positive definite.

Computing the Hessian in (40) $\left. \frac{d^2 F(Y + \epsilon \Psi)}{d\epsilon^2} \right|_{\epsilon=0} =$

$$= \sum_{i=1}^{N} \rho(i) \sum_{j=1}^{K} \pi_{Y}^{\beta}(j|i) \left[\sum_{k=1}^{K} p(k|j,i) \psi_{k}^{\top} \psi_{k} - 2\beta \left(\sum_{k=1}^{K} p(k|j,i) [y_{k} - x_{i}]^{\top} \psi_{k} \right)^{2} \right]$$
(41)

$$+2\beta \sum_{i=1}^{N} \rho(i) \left[\sum_{j,k=1}^{K} \pi_{Y}^{\beta}(j|i) p(k|j,i) [y_{k} - x_{i}]^{\top} \psi_{k} \right]^{2}$$
(42)

$$= \sum_{i=1}^{N} \rho(i) \left[\sum_{j=1}^{K} \pi_Y^{\beta}(j|i) \Psi^{\top} \left[P^{ij} - 2\beta P^{ij} z_i z_i^{\top} P^{ij} \right] \Psi \right]$$

$$(43)$$

$$+2\beta \left[\sum_{j,k=1}^{K} \pi_{Y}^{\beta}(j|i) p(k|j,i) [y_{k} - x_{i}]^{\top} \psi_{k} \right]^{2}$$
 (44)

$$= \Psi^{\top} \left[\hat{P}_{\pi_{\rho}}^{Y} - 2\beta \sum_{i=1}^{N} \sum_{j=1}^{K} P_{A}^{ij} z_{i} z_{i}^{\top} P^{ij} \right] \Psi + 2\beta \sum_{i=1}^{N} \rho(i) \left[\sum_{j,k=1}^{K} \pi_{Y}^{\beta}(j|i) p(k|j,i) [y_{k} - x_{i}]^{\top} \psi_{k} \right]^{2}$$
(45)

$$= \Psi^{\top} \left[\hat{P}_{\pi_{\rho}}^{Y} - 2\beta \sum_{i=1}^{N} \sum_{j=1}^{K} P_{A}^{ij} z_{i} z_{i}^{\top} P^{ij} \right] \Psi + 2\beta \sum_{i=1}^{N} \rho(i) \left[\sum_{j=1}^{K} \pi_{Y}^{\beta}(j|i) z_{i}^{\top} P^{ij} \Psi \right]^{2}$$
(46)

$$= \Psi^{\top} \left[\hat{P}_{\pi_{\rho}}^{Y} - 2\beta \sum_{i=1}^{N} \sum_{j=1}^{K} P_{A}^{ij} z_{i} z_{i}^{\top} P^{ij} \right] \Psi + 2\beta \sum_{i=1}^{N} \rho(i) \left[z_{i}^{\top} P^{i} \Psi \right]^{2}$$
(47)

$$= \Psi^{\top} \left[\hat{P}_{\pi_{\rho}}^{Y} - 2\beta \sum_{i=1}^{N} \sum_{j=1}^{K} P_{A}^{ij} z_{i} z_{i}^{\top} P^{ij} \right] \Psi + 2\beta \Psi^{\top} \left[\sum_{i=1}^{N} \rho(i) \left[P^{i} z_{i} z_{i}^{\top} P^{i} \right] \right] \Psi \tag{48}$$

$$= \Psi^{\top} \left[\hat{P}_{\pi_{\rho}}^{Y} - 2\beta \left(\sum_{i=1}^{N} \sum_{j=1}^{K} P_{A}^{ij} z_{i} z_{i}^{\top} P^{ij} - \sum_{i=1}^{N} \rho(i) P^{i} z_{i} z_{i}^{\top} P^{i} \right) \right] \Psi \tag{49}$$

B.2 $\beta_{\rm CR}$ - Critical annealing parameter value

The Hessian can be re-written as

$$\mathcal{H}(Y, \pi, \Psi, \beta) =$$

$$\Psi^{\top}(\hat{P}_{\pi_{\rho}}^{Y})^{\frac{1}{2}} \left[I - 2\beta (\hat{P}_{\pi_{\rho}}^{Y})^{-\frac{1}{2}} \left(\sum_{i=1}^{N} \sum_{j=1}^{K} P_{A}^{ij} z_{i} z_{i}^{\top} P^{ij} - \sum_{i=1}^{N} \rho(i) P^{i} z_{i} z_{i}^{\top} P^{i} \right) (\hat{P}_{\pi_{\rho}}^{Y})^{-\frac{1}{2}} \right] (\hat{P}_{\pi_{\rho}}^{Y})^{\frac{1}{2}} \Psi.$$

As evident from the above expression and the fact that β gets annealed from a small value to a large value, the critical $\beta_{\rm cr}$ at which Hessian loses rank is given by $\frac{1}{2\lambda_{\rm max}\left((\hat{P}_{\pi_\rho}^Y)^{-\frac{1}{2}}\Delta(\hat{P}_{\pi_\rho}^Y)^{-\frac{1}{2}}\right)}.$

C Sensitivity of Y to the annealing parameter β

Consider the expression of the cluster representatives y_{ℓ} in (2). We re-write this expression as

$$y_{\ell} = \frac{\sum_{i=1}^{N} p_{\pi_{\rho}}^{Y}(l, i) x_{i}}{p_{\pi_{\rho}}^{Y}(l)},$$

where $p_{\pi_{\rho}}^Y(l,i)=\sum_{j=1}^K \rho(i)\pi_Y^{\beta}(j|i)p(l|j,i)$ and $p_{\pi_{\rho}}^Y(l)=\sum_{i=1}^N p_{\pi_{\rho}}^Y(l,i)$. We have that

$$\frac{dy_{\ell}}{d\beta} = \frac{1}{p_{\pi_{\rho}}^{Y}(l)} \sum_{i=1}^{N} \frac{dp_{\pi_{\rho}}^{Y}(l,i)x_{i}}{d\beta} - \frac{1}{p_{\pi_{\rho}}^{Y}(l)^{2}} \sum_{i=1}^{N} p_{\pi_{\rho}}^{Y}(l,i)x_{i} \frac{dp_{\pi_{\rho}}^{Y}(l)}{d\beta}, \tag{50}$$

where $\frac{dp_{\pi_{\rho}^{Y}}(l,i)}{d\beta} = \sum_{j=1}^{K} \rho(i)p(l|j,i)\frac{d\pi_{Y}^{\beta}(j|i)}{d\beta}$, where $\pi_{Y}^{\beta}(j|i)$ is the Gibbs' distribution in (1).

$$\frac{d\pi_Y^{\beta}(j|i)}{d\beta} = -\pi_Y^{\beta}(j|i) \Big[d_{\text{avg}}(x_i, y_j) + 2\beta \sum_{k=1}^K p(k|j, i) (y_k - x_i)^{\top} \frac{dy_k}{d\beta} \Big]$$

$$+ \pi_{Y}^{\beta}(j|i) \sum_{j'=1}^{M} \pi_{Y}^{\beta}(j'|i) \left[d_{\text{avg}}(x_{i}, y_{j'}) + 2\beta \sum_{k=1}^{K} p(k|j', i) (y_{k} - x_{i})^{\top} \frac{dy_{k}}{d\beta} \right]$$
 (51)

Substituting (51) in (50), and algebraically simplifying, we obtain

$$\frac{dy_{\ell}}{d\beta} = \frac{1}{p_{\pi_{\rho}}^{Y}(l)} \sum_{i=1}^{N} \sum_{j=1}^{K} \rho(i) p(l|j, i) \pi_{Y}^{\beta}(j|i) d_{\text{avg}}(x_{i}, y_{j}) (y_{\ell} - x_{i})
+ \frac{2\beta}{p_{\pi_{\rho}}^{Y}(l)} \sum_{i=1}^{N} \sum_{j=1}^{K} \rho(i) p(l|j, i) \pi_{Y}^{\beta}(j|i) \sum_{k=1}^{K} p(k|j, i) (y_{k} - x_{i})^{\top} \frac{dy_{k}}{d\beta} (y_{\ell} - x_{i})
- \frac{1}{p_{\pi_{\rho}}^{Y}(l)} \sum_{i=1}^{N} \sum_{j=1}^{K} \rho(i) p(l|j, i) \pi_{Y}^{\beta}(j|i) \sum_{j'=1}^{K} \pi_{Y}^{\beta}(j'|i) d_{\text{avg}}(x_{i}, y_{j'}) (y_{\ell} - x_{i})
- \frac{2\beta}{p_{\pi_{\rho}}^{Y}(l)} \sum_{i=1}^{N} \sum_{j=1}^{K} \rho(i) p(l|j, i) \pi_{Y}^{\beta}(j|i) \sum_{j'=1}^{K} \pi_{Y}^{\beta}(j'|i) \sum_{k=1}^{K} p(k|j', i) (y_{k} - x_{i})^{\top} \frac{dy_{k}}{d\beta} (y_{\ell} - x_{i})$$
(52)

Multiplying (52) by $p_{\pi_{\rho}}(l) \frac{dy_{\ell}}{d\beta}$ on both the sides and summing up over all l, we obtain:

$$T_{1} := \sum_{l=1}^{K} p_{\pi_{\rho}}^{Y}(l) \frac{dy_{\ell}}{d\beta}^{\top} \frac{dy_{\ell}}{d\beta} = \sum_{i=1}^{N} \sum_{j,l=1}^{K} \rho(i) p(l|j,i) \pi_{Y}^{\beta}(j|i) d_{\text{avg}}(x_{i},y_{j}) \frac{dy_{\ell}}{d\beta}^{\top} (y_{\ell} - x_{i})$$

$$+ 2\beta \sum_{i=1}^{N} \sum_{j=1}^{K} \rho(i) \pi_{Y}^{\beta}(j|i) \left[\sum_{k=1}^{K} p(k|j,i) \frac{dy_{k}}{d\beta}^{\top} (y_{k} - x_{i}) \right]^{2}$$

$$- \sum_{i=1}^{N} \sum_{l=1}^{K} p_{\pi_{\rho}}^{Y}(l,i) \sum_{j'=1}^{K} \pi_{Y}^{\beta}(j'|i) d_{\text{avg}}(x_{i},y_{j'}) \frac{dy_{\ell}}{d\beta}^{\top} (y_{\ell} - x_{i})$$

$$- 2\beta \sum_{i=1}^{N} \rho(i) \left[\sum_{j=1}^{K} \pi_{Y}^{\beta}(j|i) \sum_{k=1}^{K} p(k|j,i) \frac{dy_{k}}{d\beta}^{\top} (y_{k} - x_{i}) \right]^{2}, \quad (53)$$

which when re-arranged gives

$$T_{1} - T_{2} + T_{3} = \sum_{i=1}^{N} \sum_{j,l,j'=1}^{K} \rho(i) p(l|j,i) \pi_{Y}^{\beta}(j|i) \pi_{Y}^{\beta}(j'|i) \left[d_{\text{avg}}(x_{i},y_{j}) - d_{\text{avg}}(x_{i},y_{j'}) \right] \frac{dy_{\ell}}{d\beta}^{\top}(y_{\ell} - x_{i}) . \tag{54}$$

Now, we'll bound some of the terms in the expression T_4 . Note that, from the expression in (1), $\pi_Y^{\beta}(j|i) \leq \exp\left\{-\beta\left(d_{\text{avg}}(x_i,y_j)-d_{\text{avg}}(x_i,y_{j'})\right)\right\}$, which implies

$$\pi_Y^{\beta}(j|i) \left(d_{\text{avg}}(x_i, y_j) - d_{\text{avg}}(x_i, y_{j'}) \right) \tag{55}$$

$$\leq \left(d_{\operatorname{avg}}(x_i, y_j) - d_{\operatorname{avg}}(x_i, y_{j'})\right) e^{\left\{-\beta \left(d_{\operatorname{avg}}(x_i, y_j) - d_{\operatorname{avg}}(x_i, y_{j'})\right)\right\}} \leq \frac{e^{-1}}{\beta}, \tag{56}$$

where the last inequality follows from the fact that $xe^{-\beta x} \le \frac{e^{-1}}{\beta}$ for $\beta > 0$. Substituting this bound in (54), we obtain

$$T_{4} \leq \frac{e^{-1}}{\beta} \sum_{i=1}^{N} \sum_{j,l,j'=1}^{K} \rho(i) p(l|j,i) \pi_{Y}^{\beta}(j|i) \pi_{Y}^{\beta}(j'|i) \frac{dy_{\ell}}{d\beta}^{\top} (y_{\ell} - x_{i})$$
 (57)

$$= \frac{e^{-1}}{\beta} \sum_{i=1}^{N} \sum_{l=1}^{K} p_{\pi_{\rho}}^{Y}(l,i) \frac{dy_{\ell}}{d\beta}^{\top} (y_{\ell} - x_{i}) \le \frac{e^{-1}}{\beta} \sum_{i=1}^{N} \sum_{l=1}^{K} \left\| \frac{dy_{\ell}}{d\beta} \right\| R_{\Omega}, \tag{58}$$

where R_{Ω} quantifies the size of the domain Ω (for instance, radius of the smallest sphere containing all the data points $\{x_i\}$). Further note from expression (42) that $T_1 - T_2 + T_3$ is essentially the

Hessian $\mathcal{H}(Y,\pi,\Psi,\beta)$ where the perturbation $\Psi = \left[\frac{dy_1}{d\beta}^\top \dots \frac{dy_K}{d\beta}^\top\right]^\top$. Thus, we have that

$$\Rightarrow \sum_{l=1}^{K} \frac{dy_{\ell}}{d\beta}^{\top} \frac{\partial^{2} F}{\partial y_{\ell}^{2}} \frac{dy_{\ell}}{d\beta} \leq \frac{e^{-1}}{\beta} N R_{\Omega} \sum_{l=1}^{K} \left\| \frac{dy_{\ell}}{d\beta} \right\|$$
 (59)

$$\Rightarrow \sum_{l=1}^{K} \lambda_{\min} \left(\frac{\partial^2 F}{\partial y_{\ell}^2} \right) \left\| \frac{dy_{\ell}}{d\beta} \right\|^2 \le \frac{e^{-1}}{\beta} N R_{\Omega} \sum_{l=1}^{K} \left\| \frac{dy_{\ell}}{d\beta} \right\|$$
 (60)

$$\Rightarrow \sum_{l=1}^{K} \delta \left\| \frac{dy_{\ell}}{d\beta} \right\|^{2} \leq \frac{e^{-1}}{\beta} N R_{\Omega} \sum_{l=1}^{K} \left\| \frac{dy_{\ell}}{d\beta} \right\|, \tag{61}$$

where $\delta = \min_l \left[\lambda_{\min} \left(\frac{\partial^2 F}{\partial y_\ell^2} \right) \right]$, and $\lambda_{\min}(\cdot)$ is the minimum eigenvalue. Note that $\sum_{l=1}^K \left\| \frac{dy_\ell}{d\beta} \right\| \le \sqrt{K} \left\| \frac{dY}{d\beta} \right\|$ by Cauchy-Schwarz inequality, where

$$\left\| \frac{dY}{d\beta} \right\| = \sqrt{\left\| \frac{dy_1}{d\beta} \right\|^2 + \ldots + \left\| \frac{dy_K}{d\beta} \right\|^2}.$$
 (62)

Thus, from (61) we have that

$$\delta \left\| \frac{dY}{d\beta} \right\|^2 \le \frac{e^{-1}}{\beta} N R_{\Omega} \sqrt{K} \left\| \frac{dY}{d\beta} \right\| \tag{63}$$

$$\Rightarrow \left\| \frac{dY}{d\beta} \right\| \le \frac{e^{-1}}{\beta \delta} N R_{\Omega} \sqrt{K} \tag{64}$$

D Change in Y versus β and Critical Temperatures

Here we illustrate how Y changes drastically near critical β_{cr} , and remains largely unchanged between two consecutive β_{cr} . Figure 3(a) illustrates the dataset that we consider for this illustration. It contains 3200 data points, and we divide it into K = 16 clusters, i.e., 16 cluster representatives $\{y_\ell\}$. Each data point has local autonomy, such that it honors the prescribed cluster 15 out 16 times, and remaining times it overrides the prescription and uniformly associates with the remaining 15 clusters. Figure 3(b) plots $\|\Delta Y(\beta)\|$ versus β . Note that change in Y remains largely zero except at 3 instances at which critical β_{cr} was attained. Initially all the representatives $\{y_\ell\}$ are coincident, i.e., all have the same feature vector values. At first β_{cr} , 4 distinct representative feature vectors value are formed, where each unique representative feature vector value is shared by 4 representatives. At the second β_{cr} each of the previous 4 unique representative vector values give rise to 2 unique representative vector value — making a total of 8 unique representative feature values at this point. Here, each unique representative feature vector value is shared by 2 representatives in $\{y_l\}$. At the third β_{cr} each of the previous 8 unique representative vectors give rise to 2 unique representative vector values — making a total of unique 16 representative vectors. See the .mp4 file "Submission-WithPT.mp4" (where plot title in every frame shows $\frac{1}{\beta}$) submitted as supplementary material for a clearer understanding.

E REINFORCEMENT-BASED LEARNING FOR CASE (C1)

Case (C1) - When \mathcal{X} contains a tractable number of data points, $d(x_i, y_k)$ is available in closed form, and p(l|j, i) is independent of y_ℓ .

Learning π_Y^{β} (S1): Our mechanism to learn the assignment policy π_Y^{β} in (1) is akin to that of learning the *control policy* in reinforcement learning (RL) frameworks (Sutton & Barto, 2018).

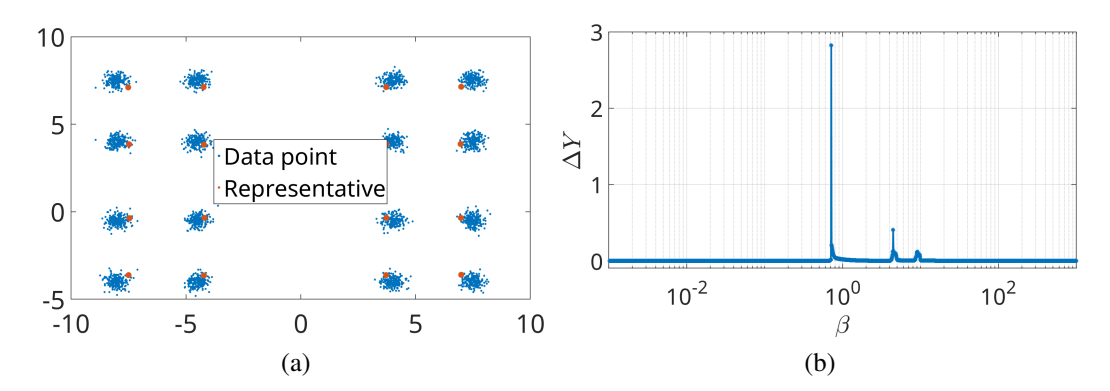


Figure 3: (a)Dataset, (b) Change in Y versus β demonstrates phenomenon of phase transitions

Let $q_t(x_i,y_j)$ be the estimate of the average cost $d_{\text{avg}}(x_i,y_j)$ at a time instant t, and $\pi_t(j|i) = \text{softmax}_j(-\beta q_t(x_i,y_j))$ be the estimate of the policy π_Y^β . At every t, we sample a data point $i \sim \rho(\cdot)$ and its prescribed cluster $j \sim \pi_t(\cdot|i)$. The data point associates itself to the cluster $k \sim p(\cdot|j,i)$ incurring a cost $d(x_i,y_k)$. We perform the following stochastic iteration to asynchronously update $q_t(x_i,y_j)$:

$$q_{t+1}(x_i, y_j) = (1 - \epsilon_{t,ij})q_t(x_i, y_j) + \epsilon_{t,ij}d(x_i, y_k), \tag{65}$$

and $q_{t+1}(x_{i'},y_{j'})=q_t(x_{i'},y_{j'})$ for all $(i',j')\neq (i,j)$. These iterations, under the Robbins-Monro step-size conditions $\sum_t \epsilon_{t,ij}=\infty$, and $\sum_t \epsilon_{t,ij}^2<\infty~\forall~i,j$, converge to the expected cost $d_{\mathrm{avg}}(x_i,y_j)$, and provide an estimate $\hat{\pi}_Y^\beta$ of the policy in (1). See (Borkar & Borkar, 2008) for proof.

Learning $\{y_\ell\}$ (S2): When the cost function $d(x_i,y_k)$ is known in the closed form and the local autonomy is not dependent on $\{y_\ell\}$, a straightforward way to learn the cluster representatives is via stochastic gradient descent (SGD). For instance, when $d(x_i,y_k) = \|x_i - y_k\|_2^2$ we execute the following SGD iterations

$$y_{\ell}(t+1) = y_{\ell}(t) - \alpha_t \left(\frac{1}{|\mathcal{S}|} \sum_{(i,j,k) \in \mathcal{S}} \left(y_{\ell}(t) - x_i \right) \delta_{\ell k} \right), \tag{66}$$

where the mini-batch $S = \{(i, j, k) : i \sim \rho, j \sim \hat{\pi}_Y^{\beta}, k \sim p\}$, and $\hat{\pi}_Y^{\beta}$ is the policy learnt in (S1).

F ADEN ARCHITECTURE

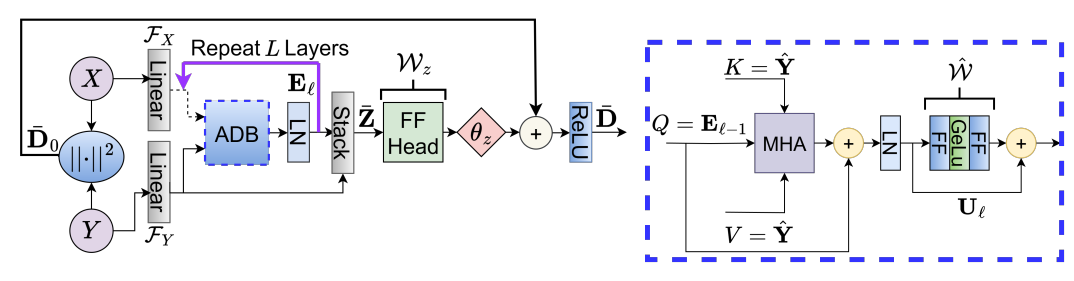
Given a set of data points \mathcal{X} and representatives \mathcal{Y} , our attention-based deep neural network NN_{θ} outputs the expected entity-cluster distance tensor

$$\bar{\mathbf{D}}_{\theta}(\mathcal{X}, \mathcal{Y}) \in \mathbb{R}_{+}^{|\mathcal{X}| \times |\mathcal{Y}|},$$

where $[\bar{\mathbf{D}}_{\theta}(\mathcal{X},\mathcal{Y})]_{ij} = d_{\theta}(x_i,y_j)$. The design of NN_{θ} allows inputs of variable sizes $(|\mathcal{X}|)$ and $|\mathcal{Y}|$, enabling efficient transfer learning across problem instances without retraining from scratch. By training $d_{\theta}(x_i,y_j)$ to approximate a target distance function $d_{\mathrm{avg}}(x_i,y_j)$, the model implicitly encodes the influence of local autonomy $p(\cdot \mid j,i)$ on the full set of cluster representatives $\{y_\ell\}$, when such dependencies exist. This design ensures that gradients with respect to the cluster representatives are accurately propagated, allowing end-to-end optimization of both entity assignments and cluster representatives.

See Figure 4 for an architecture of our proposed Adaptive Distance Estimation Network (ADEN) that incorporates an internal Adaptive Distance Block (ADB). We employ a deep encoder to estimate autonomy-aware entity-cluster distances. Suppose there are B mini-batch of data, each containing S samples and all the K clusters. We usually take $S \ll N$ to avoid computational overhead. The inputs are the data tensor $\mathbf{X} \in \mathbb{R}^{B \times S \times d}$ and the cluster tensor $\mathbf{Y} \in \mathbb{R}^{B \times K \times d}$. Both are first projected into a hidden space of dimension d_h via

$$\hat{\mathbf{X}} = \mathcal{F}_X(\mathbf{X}), \hat{\mathbf{Y}} = \mathcal{F}_Y(\mathbf{Y}),$$



(a) Schematics of ADEN Architecture.

(b) ADB Module Used inside ADEN.

Figure 4: Overall Deep Architecture to predict autonomy-aware distances.

Table 2: Hyperparameters used for different scenarios.

Parameter	Value
Seed	0
Hidden dim (d_h)	64
Feed Forward dim (d_{FF})	128
ADB Layers (L)	4
Attention Heads	8
Batch Size (B)	32
Samples in Batch (S)	128
Learning Rate (η_d)	10^{-4}
AdamW Weight Decay	10^{-5}
Perturbation spread (σ)	0.01
Sampling size (\hat{L})	16
EMA Filter rate (λ)	0.95
Epochs $Y(T_y)$	100
Learning Rate $Y(\eta_y)$	10^{-4}
β_{\min}	10
$\mid au$	1.1

Hyperparameters with different values:

Epochs ADEN (T_d)	Fig. 1 Dataset: 1000 —	Decentralized Sensing Fig 2: 2000
$eta_{ ext{max}}$	Fig. 1 Dataset: 50,000 —	Decentralized Sensing Fig 2: 10,000

where $\mathcal{F}_X, \mathcal{F}_Y : \mathbb{R}^d \to \mathbb{R}^{d_h}$ are learnable linear layers. Next, we apply L layers of ADB encoding to \hat{X} to obtain contextualized embeddings $\mathbf{E}_L \in \mathbb{R}^{B \times S \times d_h}$ (see Figure 4(b)):

$$\mathbf{U}_{\ell} = \mathrm{LN}\left(\mathrm{MHA}(\mathbf{E}_{\ell-1}, \hat{\mathbf{Y}}, \hat{\mathbf{Y}}) + \mathbf{E}_{\ell-1}\right),\tag{67}$$

$$\mathbf{E}_{\ell} = \operatorname{LN}(\hat{\mathcal{W}}(\mathbf{U}_{\ell}) + \mathbf{U}_{\ell}), \quad \ell = 1, \dots, L,$$
(68)

where $\mathbf{E}_0 = \hat{\mathbf{X}}$, MHA denotes standard multi-head attention (query, key, value), LN is layer normalization, and $\hat{\mathcal{W}} : \mathbb{R}^{d_h} \to \mathbb{R}^{d_{\mathrm{ff}}} \to \mathbb{R}^{d_h}$ is a feed-forward module with expansion–contraction linear layers $(d_{\mathrm{ff}} \gg d_h)$ and GeLU activation. To form pairwise entity–cluster features, we broadcast the final point embeddings $\mathbf{E}_L \in \mathbb{R}^{B \times S \times d_h}$ and the cluster embeddings $\hat{\mathbf{Y}} \in \mathbb{R}^{B \times K \times d_h}$ across the cluster and entity dimensions, respectively:

$$\tilde{\mathbf{E}} = \mathbf{E}_L[:,:, \text{newaxis},:] \in \mathbb{R}^{B \times S \times K \times d_h}, \qquad \tilde{\mathbf{Y}} = \hat{\mathbf{Y}}[:, \text{newaxis},:,:] \in \mathbb{R}^{B \times S \times K \times d_h}.$$

We then pairwise-combine these representations by channel-wise stacking,

$$\bar{\mathbf{Z}} = [\tilde{\mathbf{E}} \| \tilde{\mathbf{Y}}] \in \mathbb{R}^{B \times S \times K \times 2d_h},$$

where $[\cdot \| \cdot]$ denotes feature-wise concatenation for each entity-cluster pair. A shared feed-forward "distance head" $\mathcal{W}_z : \mathbb{R}^{2d_h} \to \mathbb{R}$ then predicts autonomy-aware deviations:

$$\bar{\mathbf{D}} = \text{ReLU}(\theta_z \, \mathcal{W}_z(\bar{\mathbf{Z}}) + \bar{\mathbf{D}}_0),$$

where θ_z is a learnable scalar, and $\bar{\mathbf{D}}_0$ is the baseline distance between X, Y. We define

$$ar{\mathbf{D}}_0 = \left(\mathbf{X}[:,:,\,\text{newaxis},:] - \mathbf{Y}[:,\,\text{newaxis},:,:]\right)^{\odot 2} \mathbf{1}$$

as the batched, pairwise squared Euclidean distance between \mathbf{X} and \mathbf{Y} , where $\odot 2$ denotes elementwise squaring and $\mathbf{1} \in \mathbb{R}^d$ is a vector of ones. Dropout layers within both the ADB blocks and the distance head mitigate overfitting. This design ensures permutation invariance across clusters, since \mathcal{W}_z is applied identically to every entity-cluster pair.

G ADEN TRAINING HYPERPARAMETERS

Table 2 provides the hyperparameters used for ADEN network in various simulations.

H SIMULATIONS WITH LOCAL AUTONOMY

We evaluate our method on the dataset shown in Fig. 1 under a controlled form of local autonomy. Specifically, each entity i accepts its prescribed cluster j with probability $1-\kappa$; with probability κ it selects an alternative cluster $k \neq j$ according to

$$p(k \mid j, i) = \kappa \frac{\exp[-c_k(j, i)/T]}{\sum_{t \neq j} \exp[-c_t(j, i)/T]}.$$

Here the cost $c_k(j,i) = \zeta d(y_j,y_k) + \gamma d(x_i,y_k)$. We vary the parameters $\{\kappa,\gamma,\zeta,T\}$ to study their influence on clustering outcomes. The results are shown in Fig. 5. In the visualizations, the color of each entity reflects its mixture of representative assignments, computed as a linear combination of representative colors weighted by $\pi_Y(j \mid i)$.

When κ is small (Fig. 5(a1)-(a2)), cluster representatives remain close to their assigned entities. As κ increases, deviations grow (Fig. 5(a3)-(d4)): the temperature T controls the randomness of alternative selections—higher T pulls all representatives toward a common location (Fig. 5(c1)-(c2)), whereas lower T draws each representative toward the nearest entities (Fig. 5(a1) and 5(b1)). In the high- κ regime (Fig. 5(d1)-(d4)), small T produces pronounced shifts in which representatives migrate to the closest clusters, yielding nontrivial configurations (Fig. 5(d1), 5(d3), and 5(d4)). Note how the representative on top of a cluster is not of the same colour as the data points in that cluster — highlighting the non-trivial configurations under high $\kappa=0.9$. The parameters γ and ζ further modulate assignment patterns, altering how entities distribute across representatives.

I USE OF LARGE LANGUAGE MODELS

In preparing this manuscript, we made limited use of OpenAI's ChatGPT. Specifically, ChatGPT was employed to improve grammar, clarity, and readability of the text. On rare occasions, it was also used to aid in literature discovery; however, all references and citations included in the paper were independently verified and sourced directly from Google Scholar.

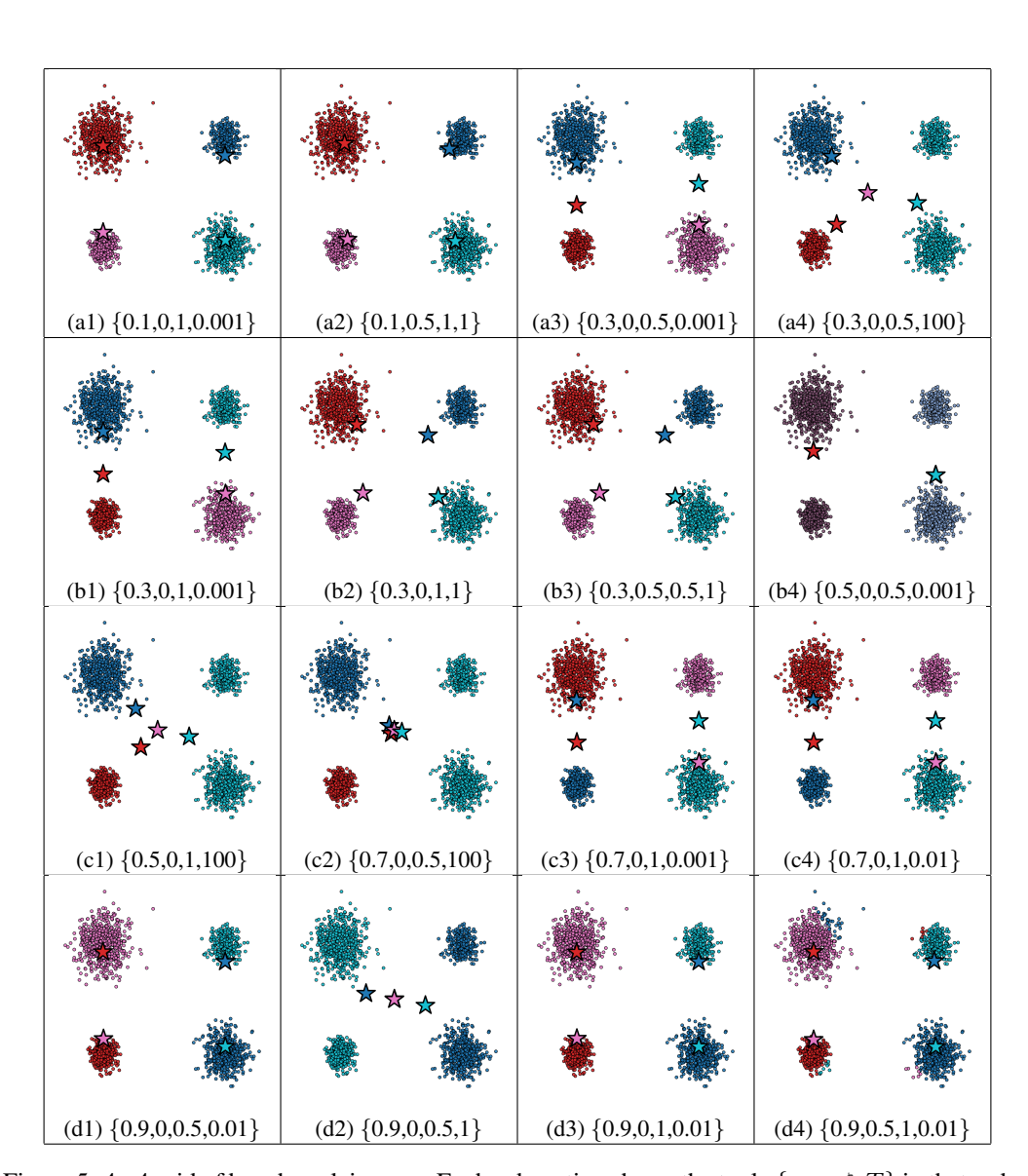


Figure 5: 4×4 grid of benchmark images. Each subcaption shows the tuple $\{\kappa, \gamma, \zeta, T\}$ in that order.